A Novel UWB RFID Tag Using Active Frequency Selective Surface

A. Lazaro, *Member, IEEE*, A. Ramos, D. Girbau, *Member, IEEE*, and R. Villarino

***Abstract*—This work describes an actively controlled frequency selective surface (FSS) to implement ultrawideband radio identification (RFID) tags. The tag exploits the change in the radar cross section (RCS) of the FSS, which is loaded with switching PIN diodes to modulate the backscattered time-domain response of the tag to an input ultra-wide band pulse. The basic operation theory of the system is explained. An experimental setup based on a ultra-wideband radar working as a reader is proposed to measure the modulated radar cross section of the tags. As a proof of concept, a battery-assisted or semipassive tag has been developed.**

***Index Terms*—Frequency selective surface (FSS), radio frequency identification (RFID), ultrawideband UWB, wake-up circuit.**

I. Introduction

ULTRAWIDEBAND (UWB) technology has been recently allowed for its commercial operation in communications. Thus, the use of UWB technology has changed dramatically in recent years [1]. In this context, UWB technology is also a promising solution for next generation radiofrequency identification (RFID) systems to overcome some of the limitations of the current narrow-band RFID technology [2], and it is also an enabling technology for future wireless sensors. UWB chipless tags for RFID systems might be a good alternative for low-cost item tagging, as recently demonstrated in [3]–[8]. Printable chipless RFID tags based on multiresonators have been reported in [3], [8], where the information is coded in frequency domain. An alternative method where the information is coded in the time delay has been proposed in [4]–[7]. However, the number of bits that chipless tags can code is small for some applications, and chip-based tags are needed. Chip-based RFID tags must receive DC power to be read. This power can come either from a battery or from the reader's signal, which is rectified to overcome a threshold voltage. The nonbattery powered chip-based tags are referred to as passive. These have a limited dynamic range determined by the regulatory limits of broadcast power and by the forward loss of signal that falls below the threshold required. In semipassive tags, battery power can be supplied to the IC in order to overcome the forward loss. Finally, active tags also use the battery power to generate and send the return signal [2].

Passive RFID tags are based on backscatter modulation, where the antenna reflection properties are changed according to the code stored in the tag. Although several frequency bands exist as a function of the application, UHF passive tags are preferred due to the compromise between price, memory capacity and distance. HF and MF frequency tags are reserved for short distances (they are based in magnetic coupling, which decreases much faster than the far field coupling used in UHF or microwave tags). However, UHF RFID technology has some drawbacks. The frequency band allocation for UHF RFID depends on the country and the read range is limited by the power transmitted from the reader, a parameter which is not the same all over the world. The read range is influenced by multipath propagation [9] and interference between readers [10]. In addition, UHF tags suffer from frequency detuning when they are attached to materials [9], [11]. Furthermore, special tags must be used in presence of metals or liquids, increasing the tag price.

Controllable electromagnetic absorption and/or reflection by materials is an important issue in the development of radar absorbing surfaces and in certain EMI/EMC problems. Conventionally, microwave materials composed by a combination of metallic and/or nonmetallic (dielectric) absorbing constituents are used for this purpose [12], [13]. The concept of facilitating such modulating capability in an electromagnetic reflecting surface is also useful in designing RFID tags [14], [15]. In this paper, the backscattering approach is based on the modulation of active controlled reflecting surface. Basically, the radar cross section (RCS) depends on the surface shape, area and materials. For instance, Fig. 1 shows a frequency selective surface (FSS) which is made by a two-dimensional array of dipoles, which in turn are loaded with switching diodes [13]. Thus, when the diodes are unbiased, they present a high-impedance state and the electromagnetic wave passes through the surface. Under these load conditions, the FSS is like an array of dipoles with half-length with respect the forward-biased case. In this case the surface presents a low RCS state (see the equivalent circuit of an FSS and the approximated current distribution shown in Fig. 2). But, when they are biased on, the diodes present a low-impedance state and the surface is like an array of rods that acts as a polarized grid, reflecting the electromagnetic waves. In this second case, the surface presents a high RCS state. Switching the diodes state, the electrical lengths of the dipoles change, resulting in modulation of the resonance frequency of the FSS. A large difference in the RCS is expected depending on the state of the diodes. Then the tag works as follows [see Fig. 3(a)]:

Manuscript received January 25, 2012; revised September 12, 2012; accepted November 09, 2012. Date of publication November 21, 2012; date of current version nulldate. This work was supported by the Spanish Government Project TEC2011-28357-C02-01.

The authors are with the Electronics, Electrical, and Automatics Engineering Department, Universitat Rovira i Virgili, 43007 Tarragona, Spain (e-mail: antonioramon.lazaro@urv.cat; angel.ramos@estudiants.urv.cat; david.girbau@urv.cat; ramon.villarino@urv.cat).

Color versions of one or more of the figures in this paper are available online at http://ieeexplore.ieee.org.

Digital Object Identifier 10.1109/TAP.2012.2228838

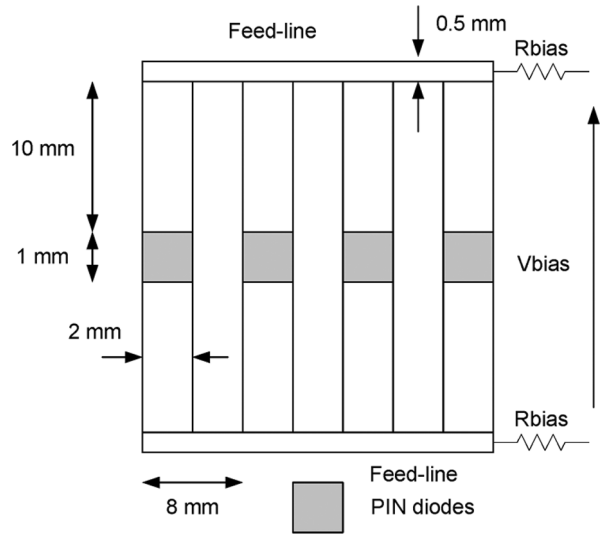

Fig. 1. Diagram of a FSS used in time-domain UWB tag including the dimensions of the manufactured FSS.

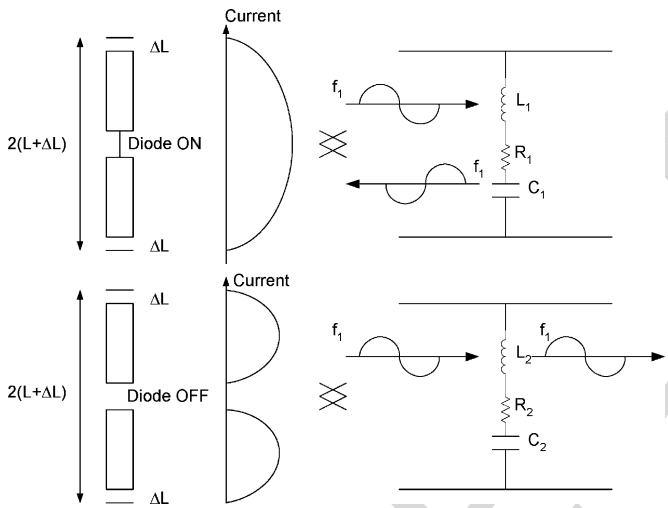

Fig. 2. Equivalent circuit model of the FSS for the two diode states. When the diode is shorted (diode ON), the waves with frequencies near the resonance frequency (f_1) are reflected, whereas the FSS is transparent for these waves when the diode is open-circuit (Diode OFF).

the reader illuminates the tag with an electromagnetic wave and part of the power is reflected due to its RCS. The information is coded in the change of the RCS due to the active elements printed on the surface of the tag.

The active reflecting surface has been used to modulate the RCS of a narrowband signal as described in [14] and [15]. But, it can also be used to modulate the amplitude of a short-time UWB pulse. This last approach is proposed in this paper. As a consequence the time-of-flight between the transmitted pulse and the modulated received pulse can be measured, permitting the localization of the tag. This feature is particularly interesting as a simple anticollision technique in dense tag scenarios, because the collected tags response can be filtered as function of the distance or its equivalent time delay. Using the UWB band allows to solve typical UHF RFID problems explained before. UWB antennas have already been used for RFID applications

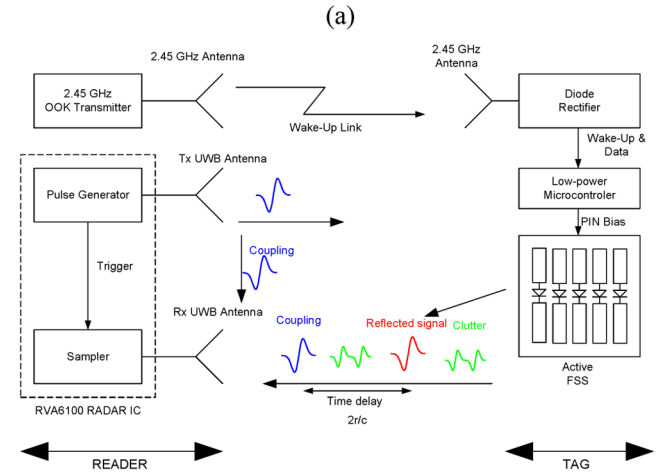

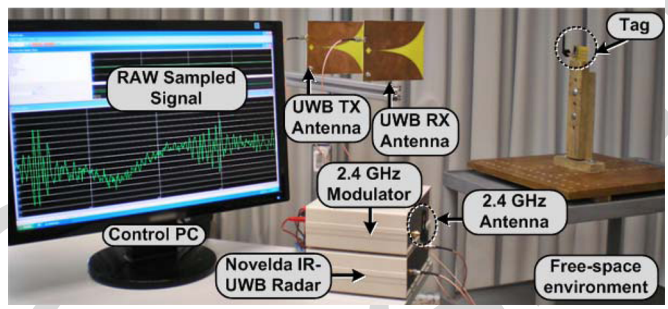

Fig. 3. (a) Block diagram schema and photograph (b) of the experimental RFID system based on a UWB radar and an FSS UWB RFID tag.

in time-domain. One approach is to code the information in the delay such as in passive chipless time-domain UWB tags [7]. Another approach consists on modulating the amplitude of the backscattering antenna mode, by changing the load impedance [5]. In this work, it is proposed to replace the UWB antenna by an active FSS. Although the communication between the tag and the reader is also done by backscattering (by modulating the load of the FSS), some important differences should be pointed out. First, the tag is illuminated by a wideband signal (UWB short pulse with wideband spectrum) instead of a CW signal. In consequence, the backscattered field on the entire pulse spectrum should be taken into account. Since FSSs are frequency-selective circuits, the reflected pulse will suffer some type of distortion. However, as it will be discussed later, it is possible to detect this pulse using standard UWB detection schemes based on matched filters or even based on energy or peak detectors [16]. For instance, in a matched filter detector, the output of the detector is proportional to the energy of the reflected pulse. Then, the key in this work is that the energy of the reflected pulse is modulated due the change in the backscattering field (and RCS) of the FSS. The FSS can be viewed as a tunable filter that filters the spectrum of the incident wideband pulse, changing the energy and also the amplitude of the reflected pulse in time domain. Second, since the RCS of an FSS increases with the number of elements, using an FSS instead of a UWB antenna can help to improve the detection of the tag. In addition, the experimental results show that it is possible to implement a low-cost UWB RFID reader using commercial UWB radars

instead of expensive instruments such as vector network analyzers or wideband oscilloscopes. In this work, an integrated UWB low-power radar from Novelda Norway [17] is used as the low-cost reader.

The paper is organized as follows. Section II deals with the basic theory of time-domain UWB RFID with active controlled FSS. Section III describes the semipassive or battery-assisted tag designed as proof of concept. The design of the active reflecting surface is given based on electromagnetic simulations. In addition, the idea of using a second radio signal to wake up the tag IC is used. Compared with previous wake-up circuits presented in the literature [18]–[20], the wake-up circuit saves power consumption because it uses the internal microcontroller comparator without the need for adding additional operational amplifiers or comparators. Section IV describes the experimental results obtained with the system. Section V draws the conclusions.

II. FSS as a UWB RFID Tag

A. Scattering Fields.

The proposed system is shown in Fig. 3. It consists of a bistatic IR-UWB radar that illuminates the tag. When the transmitted pulse hits the tag antenna, a portion of the pulse is backscattered towards the receiver. The tag consists of a FSS loaded with PIN diodes that modulate the backscattered field of the tag. In this work, an array of dipoles is considered as the FSS. Then, an active FSS can be viewed as an array of antennas loaded with the impedance of the PIN diodes. Thus, the backscattered field can be studied using fundamental antenna scattering theory [21], [22].

The backscattered field of an antenna can be split as a sum of two terms: a structural mode and an antenna mode, or a load-independent term and a load-dependent term, respectively

$$\overline{E}_s(Z_L) = \overline{E}_s(Z_{\text{ref}}) - \left(I_{\text{ref}}\overline{E}_r\right)\Gamma \tag{1}$$

where $E_S(Z_L)$ is the scattered field by the tag connected to the load Z_L, $E_S(Z_{\text{ref}})$ is the scattered field when the tag is connected to a reference load Z_{ref}, I_{ref} is the current of the antenna when connected to a load Z_{ref} and E_r is the radiated field of the antenna as a receiving antenna under a unit current source.

Depending on the author, the reference impedance can change, but often following the Green's work [22], $Z_{\text{ref}} = Z_a^*$, where Z_a is the antenna's impedance. Γ is the power reflection coefficient given by: $\Gamma = (Z_L - Z_a^*)/(Z_L + Z_a)$.

Then, the antenna reflects the structural mode when the load is the conjugate impedance of the antenna impedance. In this case, all the incident power is transferred to the load and the antenna only reflects the structural mode. The structural mode arises from the induced current on the antenna conducting surface by the incident wave, and it does not depend on the load. The structural mode depends on characteristics such as the antenna type, geometry, and material. Thus, the structural mode is independent of the load reflection coefficient, whereas the antenna mode is proportional to it.

The radar cross-section of a target is a far-field quantity that can be expressed by using (1) as

$$\text{RCS} = \left|\sqrt{\text{RCS}_{\text{struc}}} + \sqrt{\text{RCS}_a}e^{j\varphi_{as}}\right|^2 \tag{2}$$

where $\text{RCS}_{\text{struc}}$ is the RCS due to structural mode, RCS_a is the RCS due to antenna mode (which depends on the load), and ϕ_{as} is the phase difference between these two modes.

In conventional narrowband RFID systems the incident continuous wave (CW) at the tag antenna is modulated by changing the tag's load between two values. The received power for each state is proportional to the RCS given by (2). In passive RFID systems, the mean power between the two states should be greater than a minimum threshold power in order to obtain the enough DC power for the chip operation. As most RFID readers use coherent receivers, the bit error rate (BER) is a function of the difference between the backscattered fields for the two states. In consequence, the BER is optimized by maximizing the differential RCS, as defined by [23]

$$\text{RCS}_{\text{dif}} = \frac{\lambda^2}{4\pi}G^2|\Gamma_{\text{on}} - \Gamma_{\text{off}}|^2 = \frac{4\pi}{\lambda^2}A_{\text{ef}}^2|\Gamma_{\text{on}} - \Gamma_{\text{off}}|^2 \tag{3}$$

where A_{ef} is the effective area of the antenna, Γ_{on} and Γ_{off} are the reflection coefficients of the antenna load (i.e., chip) for each bit state, and λ is the wavelength. The structural component A_s is often omitted during the tag design process [23], claiming that this term does not influence the BER performance of the system, since it is common in the backscattered field, regardless of the connected load.

The RCS of a FSS depends on the frequency and its reflectivity. When the frequency of the incident wave is close to the dipoles resonance frequency (when the dipoles become approximately half wavelength [13]), the FSS presents a high reflectivity. This reflectivity is close to 1 at its resonant frequency. Thus, an important issue is that the RCS of an FSS of area A, near its resonance frequency, is proportional to the RCS of a flat plate (in optical region and with normal orientation) with the same area [12], [13].

Considering an FSS as an array of antennas, it can potentially be used to improve the detection of tags in traditional narrowband backscattering RFID systems. If the distance between the elements of the FSS is small compared to the operating wavelength, the gain is approximately equal to the gain of one single element multiplied by the number of elements in the FSS (assuming there is not a polarization mismatch and the FSS is oriented to the reader). This fact is also used in grid arrays of tags proposed in [15] to improve the reading range and tag gain.

B. Tag Detection

In order to design a UWB tag based on an FSS it is important to understand the interaction between the radar and the tag in time domain. In the case of a free-space channel and assuming a monostatic reader, the received signal is written in the frequency domain as

$$S(\omega) = H_{\text{TX}}(\omega)H_{\text{CH}}(\omega, r)\frac{\sqrt{\text{RCS}}e^{j\phi}}{\lambda} \times H_{\text{CH}}(\omega, r)H_{\text{RX}}(\omega)P(\omega) \tag{4}$$

where ϕ is the phase of the backscattered signal, ω is the angular frequency, $P(\omega)$ is the Fourier transform of the transmitted pulse and the free-space channel transfer function $H_{\rm CH}$ is given by [24], [25]. In practice, the channel transfer function $H_{\rm CH}$ in (4) can be characterized from the measured $\rm S_{21}$ parameter as a function of the frequency using a Vector Network Analyzer (the TX antenna is connected to port 1, and the RX one to port 2). Moreover, the product $H_{\rm TX}(\omega)H_{\rm CH}(\omega)H_{\rm RX}(\omega)$ can be obtained from the Fourier transform of the received time domain signal $(s_{\rm cal}(\rm t))$ measured by the radar receiver when the TX and RX antennas are oriented face-to-face and spaced a distance $r_{\rm cal}$

$$S_{\rm cal}(\omega) = \Im(s_{\rm cal}(t)) = H_{\rm TX}(\omega)H_{\rm CH}(\omega, r_{\rm cal}) \times H_{\rm RX}(\omega)P(\omega). \quad (5)$$

Then, the received signal as function of the frequency can be written as

$$S(\omega) = S_{\rm cal}(\omega)\frac{r_{\rm cal}}{r}e^{-jk(r-r_{\rm cal})}H_{\rm CH}(\omega, r)\frac{\sqrt{\rm RCS}e^{j\phi}}{\lambda}. \quad (6)$$

Finally, the received signal in time domain $(s(t))$ can be obtained from the Inverse Fourier transform of $S(\omega)$.

From the previous discussion it is expected an important difference in the level of the reflected signal by the FSS as a function of the load impedance. It can be observed that the amplitude of the received signal when the FSS is loaded with an open-circuit (diodes OFF) is much lower than when the FSS is loaded with a short-circuit (diodes ON). This makes possible to use the FSS to modulate the amplitude of UWB pulses. Unfortunately, the difference in the RCS between the ON and OFF diodes states is smaller than in the ideal case, mainly due to the effect of diode parasitic elements, as it will be studied in Section III.

Common UWB detection methods can be used to demodulate the received pulse $s(t)$. The most simple is a peak detector. Since the amplitude of the received pulse is a function of the backscattering field at each state of the FSS, a threshold comparator can be used to demodulate the signal. Other common technique is using a matched filter or a correlator. In this approach, the received signal is correlated with a stored template. The output of this detector is proportional to the energy of the received pulse. This energy can be computed by using the Parseval's theorem and (4)

$$E = \int_{-\infty}^{+\infty}|s(t)|^2dt = \frac{1}{2\pi}\int_{-\infty}^{+\infty}|S(\omega)|^2d\omega. \quad (7)$$

It can be noted that the energy does not depend on the phase ϕ of the backscattered signal. The peak detector and the matched filter methods, however, have some problems. The mached filter maximizes the signal to noise ratio in the sampling instant if the template signal is the same (or proportional) to the received pulse. In practice, the shape of the received pulse due to the distortion introduced by the reader's Tx and Rx antennas, as well as the FSS frequency response, may be difficult to know *a priori*. A solution to this problem may be to use the technique proposed by the authors in [7] using a Wavelet decomposition as a bank of matched filters. Another issue in both detectors is the need to remove the received pulses due to multipath components caused by reflections in objects near the tag. This can be done by substracting a previously stored signal without the presence of the tag, called background subtraction. This calibration can be easily done if the environment is stationary and the surrounding objects do not change their position around the tag with the time. Unfortunately, this is not the real case, since an RFID reader can move its position, which requires a periodic calibration. To solve this problem, a differential approach is proposed in this work. The information can be coded in the change of states. The differential signal considered is the substraction between each signal and a previously stored received signal (which can be the signal corresponding to the first bit of a short sequence, or the signal corresponding to the immediately previous bit). The background and clutter multipath components will be removed, since they will be the same for both states. This assumption is reasonably certain if high or moderate transmission rates are used, because the reference signal has very similar background and clutter components. The differential signal is proportional to the difference between two backscattering fields and it can be obtained calculating the difference for the two states using (6). Similar to narrow band RFID systems, this difference can be expressed as function of the differential RCS

$$S_{\rm dif}(\omega) = \Delta S(\omega) = S_{\rm cal}(\omega)\frac{r_{\rm cal}}{r}e^{-jk(r-r_{\rm cal})} \times H_{\rm CH}(\omega, r)\frac{\sqrt{\rm RCS_{dif}}}{\lambda}. \quad (8)$$

Again (8) does not depend neither on phase ϕ or on the structural mode. These differential schemas are compatible with mached filter (or Wavelet detection) approaches because the template is a previously received signal. However, as it will be shown in the results, a simple envelope detector with a comparator can be used instead of these approaches.

III. Tag Design

As a proof of concept, a semipassive tag has been designed (see Fig. 4). The tag is composed by the following blocks [as shown in Fig. 3(a))]: a diode rectifier (to obtain a 2.4 GHz tone wakeup signal from the reader), a low power microcontroller, and an active FSS. Recently, ultra-low power microcontrollers have been commercialized by Microchip. The PIC 16F1827 [26] is selected for this design. It consumes less than 100 nA in sleep mode, and 210 μA at a 1 MHz clock. The tag is powered by a 3 V Lithium battery. In wireless sensor networks, the tag is normally inactive for long time periods [18]. During these time intervals the microcontroller rests in sleep mode (low-power consumption state), and it only wakes up when it receives a wakeup signal from the reader or periodically to acquire a sensor measurement. The life of the battery depends on the time the receiver and transmitter are active.

A. Wake-Up Circuit

Wakeup radio avoids the complex bookkeeping associated with energy-efficient MAC protocols, but at the price of additional hardware [18]–[20]. So that a receiver can fire up its

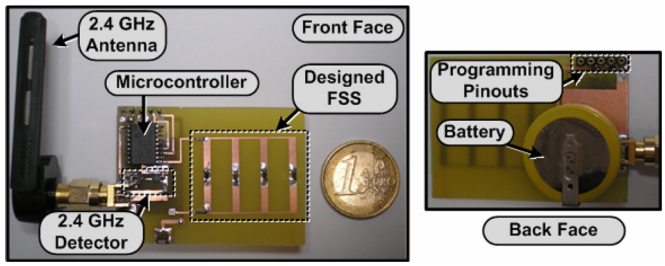

Fig. 4. Photograph of the designed tag, front (left) and back (right).

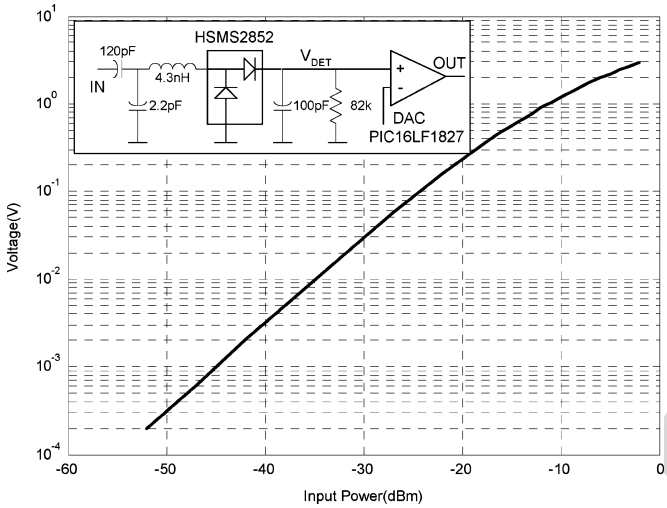

Fig. 5. Wake-up and data demodulator based on a Schottky diode detector and measured voltage detected for the designed detector.

primary radio to engage in efficient high-speed communication with the sender. In our case, a 2.45 GHz Schottky diode-based detector is used as the receiver. The reader sends an on-off-keying (OOK) modulated signal to wake up the tag. In order to prevent random wake up due to in-band interference from other systems, the tag only wakes up when a previously known stored bit sequence is received. This sequence can be considered as an address to select a specific tag or sensor within a wireless sensor network. The diode detector schema is shown in Fig. 5. It is composed by a LC matching network tuned at 2.45 GHz and two zero bias diodes in series configuration (Avago HSMS-2852) [27]. The output of the diodes is filtered by a parallel RC network and it is directly connected to an internal comparator of the microcontroller. The voltage threshold of the comparator is configurable via the internal digital-to-analog converter (DAC) of the microcontroller. This fact allows a tunable minimum wake-up distance without adding additional components to the tag, saving power consumption and protecting from unintended wake ups. When this threshold is exceeded by the rectified signal, the microcontroller executes an interrupt routine. Then, it sends the stored data (an identification code) by changing the voltage of the PIN diodes that load the FSS. After this process, the microcontroller returns to sleep mode to increase the battery life time.

The maximum read range obtained with this demonstrator is about 2 meters, thus the 2.45 GHz ISM band allows an EIRP up to 27 dBm (for outdoor mode in Europe). If a higher wake-up

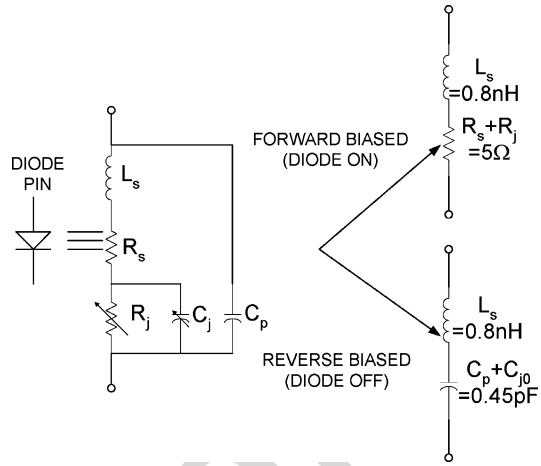

Fig. 6. High frequency equivalent circuit for the PIN diode used.

distance is required, the UHF RFID band can be used, since a higher maximum transmitted power is available (0.5 W under ETSEI EN 300 220 or 2 W under ETSI EN 302 208, and 4 W under FCC in US). The band change can be done with a simple modification of the tuned LC matching circuit. Fig. 5 shows the measured detected voltage ($\mathrm{V_{DET}}$) as a function of the power level for an input tone at 2.45 GHz. The detector sensitivity is adjusted to about -40 dBm by setting the threshold voltage to 3 mV in the comparator using the DAC. This sensitivity corresponds to a distance higher than 10 m using a dual-polarized patch antenna which transmits a 20 dBm EIRP, and a dipole antenna in the tag. Thus, the read range in our demonstrator is limited by the UWB down-link rather than the 2.45 GHz wake-up link.

B. FSS Design

The FSS is designed using a low-cost 1.6 mm thick FR4-Epoxy substrate (relative permittivity $\varepsilon_\mathrm{r} = 4.4$, loss tangent $\tan\delta = 0.02$). High frequency PIN diodes are one of the most commonly used active elements applied to reconfigure the EM response of a FSS surface [12], [13], [28]. Fig. 6 depicts the applied electrical circuit model of the BAP51-03 PIN-Diode [29] in the simulation [29], [30] for the two-states. In the forward biased case, the diode mainly represents a small resistance, which has small effect on the desired response of the FSS surface. Because of its small value, the series self inductance of the diode in this case should be considered for simulations in UWB. However, when it is reverse biased, the parasitic capacitance considerably deviates the position of the surface stop-band by altering the total effective capacitance of the unit cell. Therefore, it is required to consider its effect in the design process.

The length of the dipoles is chosen to resonate at the peak frequency of the transmitted UWB pulse (about 4 GHz) when the diodes are forward biased (approximately loaded with a short circuit). When the diodes are reverse biased, their impedance is approximately equal to the parasitic capacitance C_p plus a junction capacitance C_{j0} ($C_p + C_{j0} = 0.45$ pF), in series with a 0.8 nH parasitic inductance L_s. Thus, an important shift in the resonance frequency of the FSS is expected in the reverse biased state. It is not trivial to compute the exact circuit parameters of

the FSS, and in practice a numerical approach is necessary [12], so FEKO using Multilevel Fast Multipole Method (MLFMM) has been used to carry out the numerical simulations. The diodes are modeled using lumped elements such as the ones shown in Fig. 6. The dimensions of the FSS designed are shown in Fig. 1. The FSS is composed by four printed dipoles with 20 mm length and 2 mm width. The feed lines width is 0.5 mm, and the spacing between the dipoles is 8 mm. The diodes are biased using high impedance transmission lines connected to the bias resistor to limit the current. The feed lines are connected at the end of the dipoles, presenting a high impedance in order to not change the current distribution, in constrast with an ideal dipole which presents an open circuit at these points. To avoid increasing the number of resistors, the bias resistors are connected at the end of the feed lines (see *Rbias* in Fig. 1). As the impedance associated to the parasitic inductance dominates over the diode resistance and to limit the power consumption, the diodes are biased at 0.5 mA in forward conditions ($V_{\text{bias}} = 3$ V, $R_{\text{bias}} = 2.3$ kΩ).

Fig. 7 shows the RCS of the FSS for different load conditions. This figure compares the RCS for the FSS loaded with an ideal short-circuit ($Z_L = 0$), an ideal open-circuit ($Z_L = \infty$), when the PIN diodes biased on ($I = 0.5$ mA, $Z_L = j\omega 0.8$ nH $+ 5$) and when it is in reverse bias ($V = 0, Z_L = j\omega 0.8$ nH $+ 1/(j\omega 0.45$ pF$)$). A great difference in the RCS between short and open circuit load conditions is observed in the frequency band of the UWB radar (1–4.5 GHz). However, due to the diodes parasitic capacitance, the shift in the FSS resonant frequency is reduced. The difference between the RCS states is also reduced. In order to investigate the effect of the feed lines, Fig. 8 shows the simulation for the same load conditions of four dipoles without the feed lines. We observe a change in the shape of the resonance. But in the frequency range of interest the change is not very significant for our purposes. In both cases, the bandwidth of the resonance is higher than in free space as an effect of the dielectric thickness [12]. Fig. 9 shows the simulated RCS for a single printed dipole. The dimensions of the dipole are the same than the ones for a dipole element in the FSS of Figs. 7–8. It can be observed that the bandwidth of the FSS is larger than the dipole antenna. The peak of the RCS at the resonant frequency in the case of the FSS is higher than in the case of the dipole antenna. Figs. 10–12 show the phase of the backscattered field of the tag including the feed lines, without the feed lines and with a printed dipole antenna, respectively. In all the cases, at low frequency the phase is close to 180°. In this frequency range, the FSS acts as a metallic reflector because the separation between the rods is small compared with the wavelength. The phase decreases faster when the frequency is close to the resonant frequency of the dipoles. According to the equivalent circuits of Fig. 2., the resonant frequency of a FSS loaded with an open circuit is about the double than when it is loaded with a short circuit. So, important differences in the backscattering phase can be shown between open and short circuit load conditions. Due to the parasitic effect of PIN diodes, the change in the load impedance is not greater than between open and short circuit conditions, resulting in a similar backscattering phase behavior.

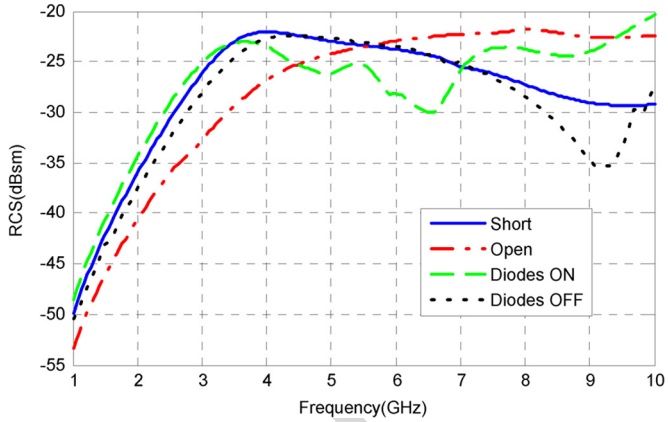

Fig. 7. Simulated RCS of the tag including feed lines.

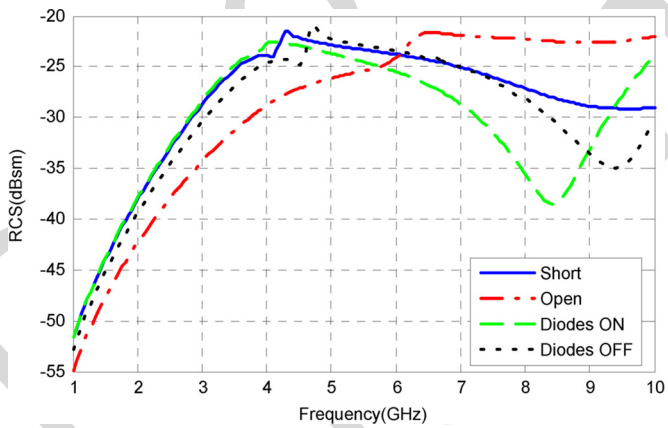

Fig. 8. Simulated RCS of the tag without the feed lines.

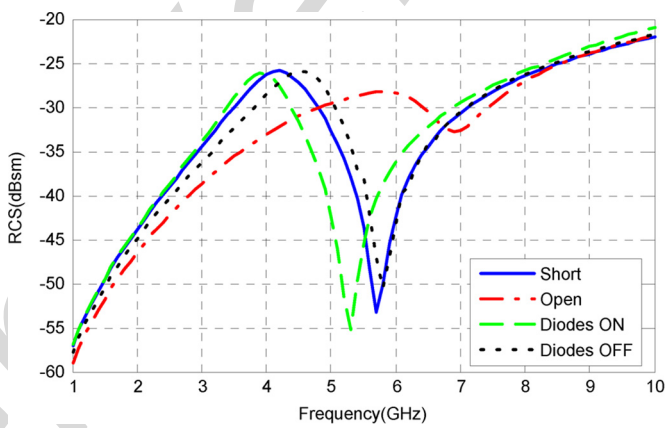

Fig. 9. Simulated RCS of a printed dipole.

From the last simulations the energy reflected by an FSS due its higher bandwidth will be higher than for a single dipole antenna. Also, the reflected pulses will suffer less distortion.

As explained before, if a differential detector is used, the received signal is a function of the differential RCS. From the scattering field given by (1) for short ($\Gamma = -1$) and open ($\Gamma = 1$) load conditions ($E_s(0)$ and $E_s(\infty)$, respectively), it is possible to separate the structural mode $E_S(Z_{\text{ref}})$ and the antenna mode, which is proportional to $(I_{\text{ref}} E_r)$

$$\overline{E}_s(Z_{\text{ref}}) = (\overline{E}_s(0) + \overline{E}_s(\infty))/2 \qquad (10)$$

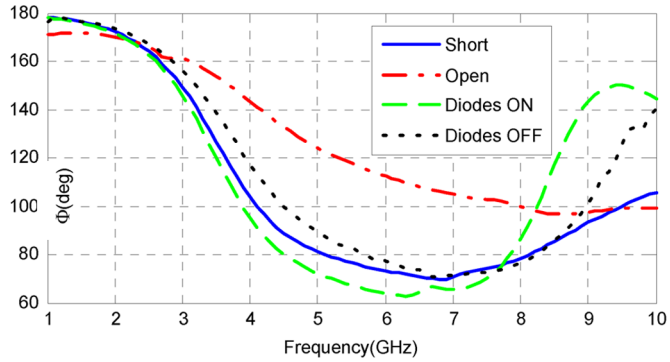

Fig. 10. Phase of the backscattered field of the tag including feeding lines.

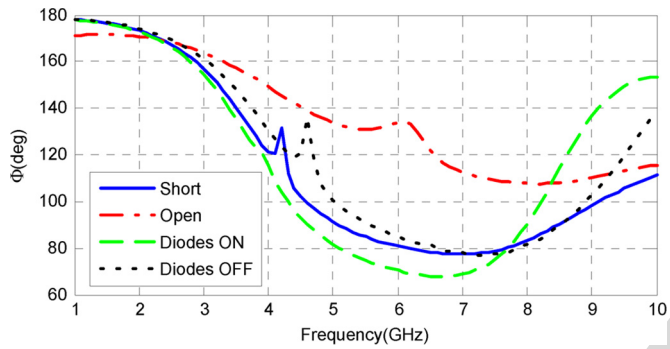

Fig. 11. Phase of the backscattered field of the tag without the feeding lines.

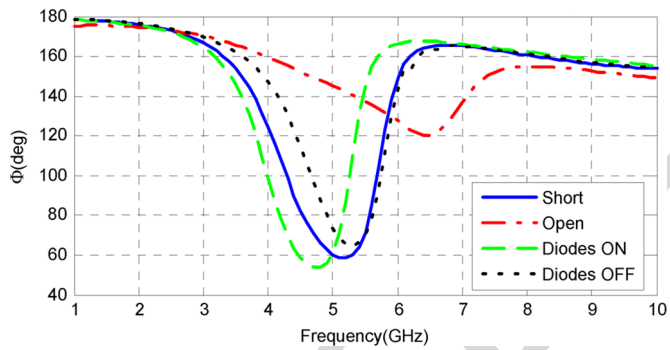

Fig. 12. Phase of the backscattered field of the printed dipole.

$$I_{\mathrm{ref}}\overline{E}_r = (\overline{E}_s(0) - \overline{E}_s(\infty))/2. \qquad (11)$$

Fig. 13 investigates the frequency behavior of the structural and antenna modes for open and short load conditions (term $\mathrm{I_{ref}E}_r$) for the FSS designed. This figure compares the differential RCS obtained from the difference in the backscattering field for ideal short and open conditions and with the diodes in ON and OFF states. It can be observed that the structural mode for frequencies below the resonance is higher than the antenna mode. For frequencies greater than the resonance frequency, the antenna mode is the one that predominates. Depending on the phase of the load reflection coefficient, the sum can be constructive or destructive. So, the differential RCS between short and open load conditions is often higher than for other load conditions. Fig. 14 repeats the study for a printed dipole antenna. Finally, Fig. 15 compares the differential RCS for the FSS and the

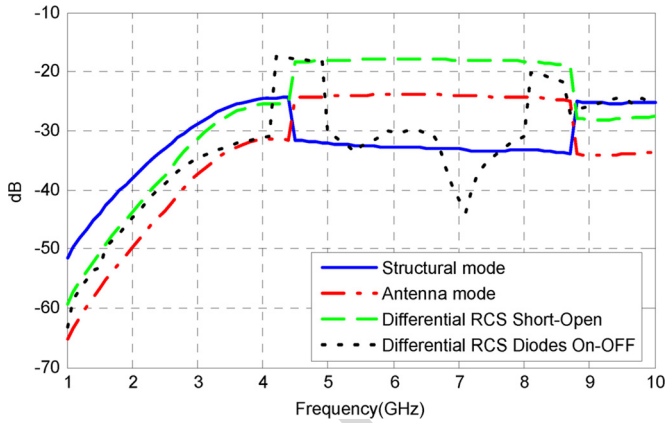

Fig. 13. FSS case: Structural mode and antenna mode for open condition, and differential RCS between Short-Open states and between Diodes ON-OFF states.

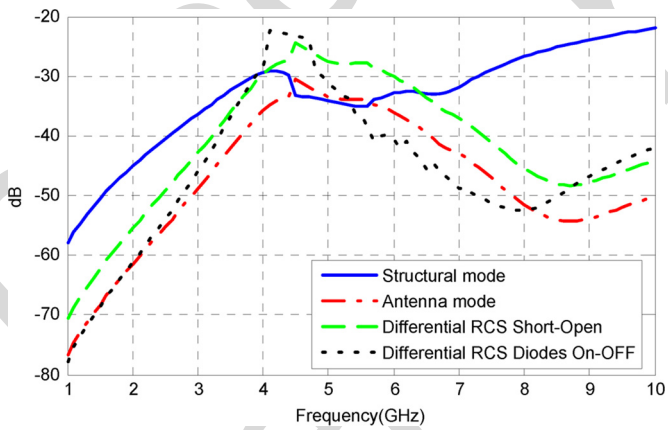

Fig. 14. Dipole case: Structural mode and antenna mode for open condition, and differential RCS between Short-Open states and between Diodes ON-OFF states.

printed dipole antenna. For the ideal short and open load conditions a considerable higher differential RCS in a large bandwidth is obtained. Using the PIN diodes, however, it is difficult to obtain such large difference between the two states. Thus, in the realistic case of the FSS and dipole antenna loaded with the PIN diodes, the bandwidth is reduced due the proximity between the reflection coefficients for the two states.

IV. Experimental Results

The experimental setup is shown in Fig. 3. The Novelda NVA6100 IC [17] is used as the reader. The NVA6100 is a fully-integrated nanoscale impulse radar transceiver, designed for low-power applications. Rather than continuously sampling the received signal, the NVA6100 employs a concept known as strobed sampling, which is described in [31]. For each pulse transmitted, the backscattered EM energy is sampled after a given time offset. This offset represents the time-of-flight of the signal relative to the time of transmission, which in turn can be used to represent the distance to the remote object. In order to avoid the Maximum Unambiguous Range limitation, a staggered pulse repetition frequency (PRF) has been used [31]. The radar generator transmits a near-Gaussian monocycle of

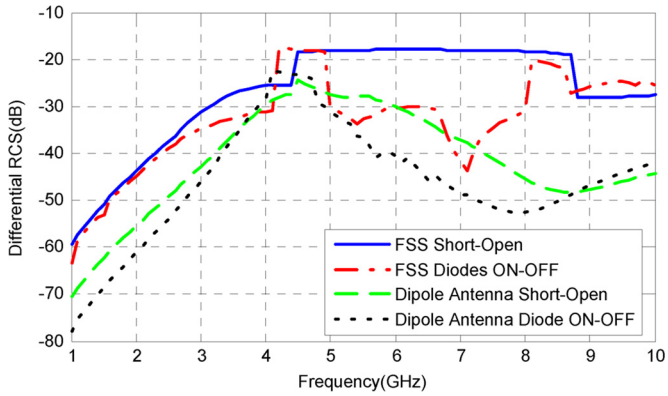

Fig. 15. Comparison of the differential RCS between the FSS and a dipole antenna between Short-Open states and between Diodes ON-OFF states.

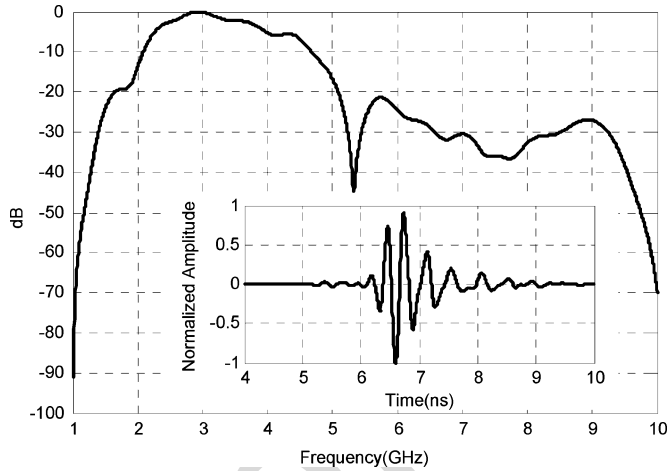

Fig. 16. Frequency response of the transfer function. In the inset figure the measured time response.

about 0.8 Vpp amplitude, 4.4 GHz center frequency and 125 ps duration.

In order to predict the modulating index of the OOK modulation from the simulated RCS, the overall transfer function is needed $H_{\mathrm{TX}}(\omega)H_{\mathrm{CH}}(\omega)H_{\mathrm{RX}}(\omega)$. Using the method described in Section II, the transfer function (when measured with the antennas oriented face-to-face) can be obtained from the received signal. In our case, two identical Vivaldi antennas excited with microstrip-to-slot line transition are used as TX and RX antennas. These antennas are often used in UWB applications and present moderate gain and low distortion. The antennas are a scaled version of the antenna presented in [32]. These antennas have a VSWR typically better than 2 and a bandwidth between 1.4 and 8.8 GHz. Fig. 16 shows the normalized transfer function as a function of the frequency. The inset plot shows the normalized time-domain measured signal $(s_{\mathrm{cal}}(t))$. There is a clear band-pass effect as a consequence of the combination of the pulse band-pass spectrum and the antenna transfer function. Thus, the amplitude of the reflected pulse on the FSS depends on the RCS apodized by this band-pass function. Fig. 17 shows the time-domain signal reflected by the FSS for different load conditions. These signals are obtained by the Fourier inverse transform of the product of the backscattered field obtained from Figs. 7 and 10, and the transfer function given in Fig. 16. Fig. 18 shows that a simple envelope detector (for instance by the modulus of the Hilbert transform of the time-domain signal) can be used to demodulate the OOK signal. As explained in Section II, the diodes parasitic elements reduce the transparence of the FSS. An amplitude modulating index close to 0.5 can be achieved between short and open circuit load conditions. However, due to the reduction in the FSS transparence for the state with the diodes in OFF, the modulating index is close to 0.85 between the ON and OFF states. In order to interpret these results, the FSS must be viewed as a bandpass filter. The amplitude of the reflected energy and in consequence the amplitude of the reflected pulse is higher for short load conditions and when the diodes are ON. For these cases, the resonance frequency of the FSS has approximately the same frequency than the peak of the spectrum of the pulse. Whereas in the case of diodes OFF and specially for open load condition due to the shift of the FSS resonance frequency, the reflected energy is smaller than on short and diodes ON cases. So, the level of the reflected signal is a

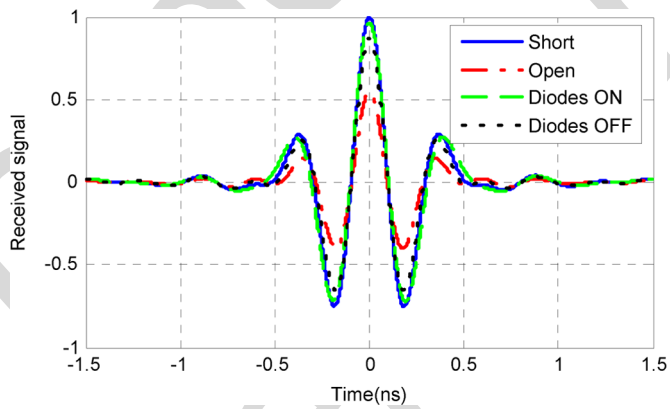

Fig. 17. Simulated normalized received signal as function of time for different load conditions.

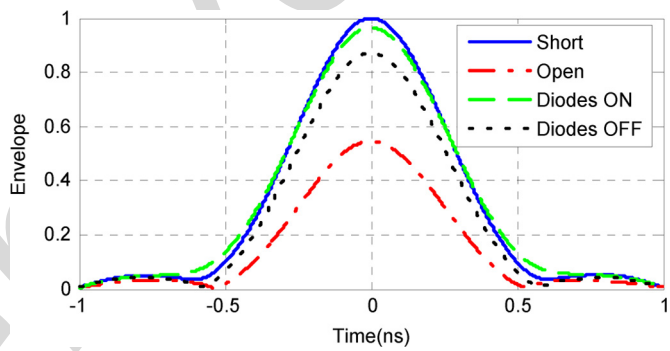

Fig. 18. Simulated normalized envelope of the time-domain response of tag.

function of the offset between the FSS frequency pass bands between states.

Figs. 19 and 20 show the measured reflected signal by the tag for tag-to-reader distances of 0.5 and 1.5 m, respectively. In both cases, the radar receives 512 time samples spaced approximately 30 ps between each sample. A time offset can be configured to choose the measurement range window. At the top of Figs. 19 and 20 the envelope of the raw signal is shown. The presence of strong clutter from the ground reflections is observed because the measurements are done in a real scenario, not

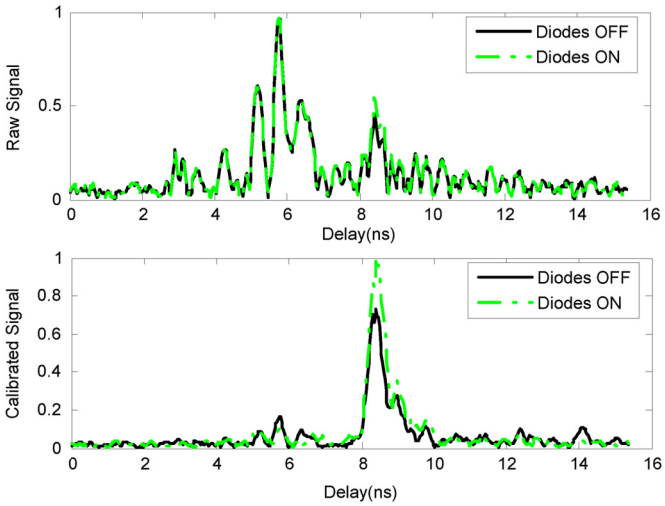

Fig. 19. Envelope of the measured signal (top), and the envelope of the signal after background removed (bottom) from the tag-to-reader distance of 0.5 m.

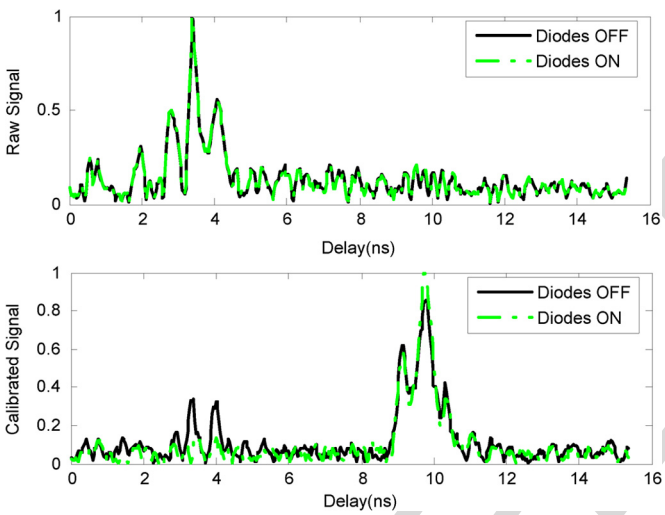

Fig. 20. Envelope of the measured signal (top), and the envelope of the signal after background removed (bottom) from the tag-to-reader distance of 1.5 m.

in an anechoic chamber. After removing the background previously measured (measurement without the tag), the tag response can be clearly viewed at the bottom of Figs. 19 and 20. The measured modulating index is very close to the simulated one (about 0.8).

In order to evaluate the distortion of the received pulse due to the FSS, Fig. 21 compares the measured received pulses reflected by a large metal plate (assumed as the reference) and the reflected pulse by the FSS in its two states. The same pulse generator than in Fig. 16 has been used. It can be seen that the shape is not much changed. The fidelity factor [33] is often used to measure the distortion due to shape changes. In this case, taking as the reference the pulse reflected by the metal plate, the fidelity factors are 0.94 and 0.98 for the OFF and ON states, respectively. Therefore, the FSS can support (with low distortion) typical UWB pulses with a centre frequency between 3 and 4 GHz.

The next figures show the measured signal when a sequence of bits is sent by the tag modulating the backscattered signal.

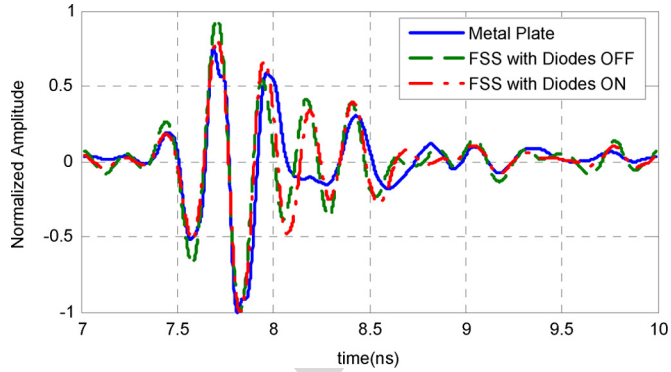

Fig. 21. Measured time domain received signal for a metal plate target and the FSS with Diodes OFF and ON.

The bit 0 is obtained when the diodes are OFF and the bit 1 when the diodes are ON. At the top of Fig. 22 the envelope of the received signal is shown. To demodulate the sequence, it is possible to use a simple threshold comparator. However, this method requires the adaptive estimation of the threshold, since it changes with the tag-to-reader distance. In addition, as explained before, this method needs to solve the problem of the estimation of the background in real RFID scenarios. An improvement can be obtained if differential coding is used. Assuming that the tag remains in repose, the first bit is zero because the diodes are OFF. Then, the measured waveform for the first bit can be used as an estimation of the background that will be subtracted in the next bits. Fig. 22 (bottom) shows the envelope of the differential signal. Thanks to the high repeatability in the bit states a simple threshold can be obtained to demodulate the sequence (i.e., by setting the threshold to equal the half of the maximum normalized envelope amplitude). Figs. 23 and 24 show an image of the envelope as a function of the delay for each bit of the sequence, before and after subtracting the first bit waveform (differential schema), respectively. It can be observed that the "0" and "1" signals are more distinguishable between each other when the differential schema is applied.

V. Conclusion

In this work, the basic theory of operation of UWB RFID using active FSS as tags has been presented. The results show that is possible to modulate the amplitude of the time-domain backscattered signal using a simple FSS. The FSS is composed by printed dipoles loaded with PIN diodes as switching elements. In contrast with traditional backscattering methods where the tag or antenna mode is modulated, in this work the total radar cross section of the surface (equivalent to the structural mode in antennas) is modulated. The RCS is proportional to the area and increases with the wavelength facilitating the tag detection. The index of modulation depends largely on the diode parasitic elements. However, the detection of the backscattered signal can be done using differential schemas that remove clutter interferences in the signal without using advanced calibration or threshold estimation techniques. A semipassive tag has been designed as a proof of concept. The tag integrates a low-power microcontroller. The tag remains in sleep mode with ultra-low power consumption until a 2.45

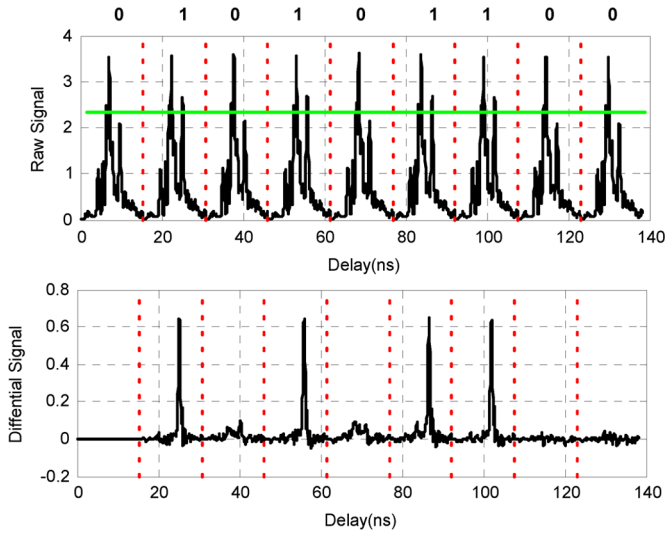

Fig. 22. Envelope of the received signal (top figure) and the differential signal obtained subtracting the waveform for the first bit (bottom figure), for the bit sequence shown in the top. The tag-to-reader distance is 0.5 m.

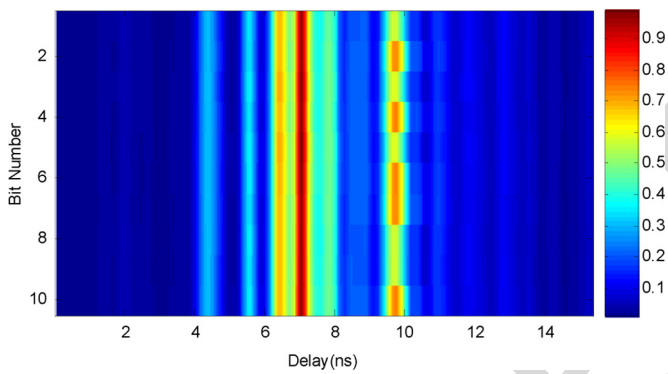

Fig. 23. Image of the envelope of the received signal for the same bit sequence of Fig. 22.

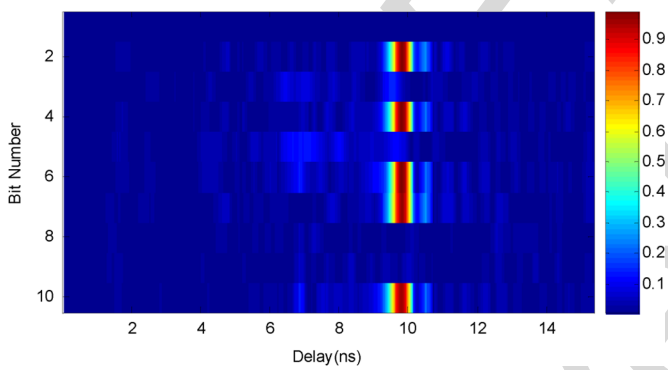

Fig. 24. Image of the envelope of the differential signal for the same bit sequence of Fig. 22.

GHz modulated signal wakes up the tag. The wake-up circuit is based on a diode detector and it uses the microcontroller comparator to reduce the number of parts and the consumption. Then, the microcontroller transmits the stored data or identification data modulating the RCS of the FSS. An experimental setup based on a low-power UWB radar is used as the reader. These results open the door to use FSS technologies in UWB RFID applications such ultra-low cost and ultra-low power environmental sensor networks.

Ranging and positioning are other benefits that UWB scheme brings to the system. It can be a powerful candidate for asset monitoring and positioning applications. The use of backscattering system allows reduce the power compared with active or semi passive tags based on ASK or FSK transmitters. In addition, these tags can be read by low power UWB radar in contrast with narrow band traditional passive RFID systems where high transmitted power and high power consuming readers are required.

ACKNOWLEDGMENT

The authors would like to thank Prof. Josep Parrón from Telecommunication and System Engineering Department of the Universitat Autònoma de Barcelona (UAB) for his support with the electromagnetic simulations with FEKO.

REFERENCES

[1] R. J. Fontana, "Recent system applications of short-pulse ultra-wideband (UWB) technology," *IEEE Trans. Microw.Theory Tech.*, vol. 52, no. 9, pp. 2087–2104, Sep. 2004.

[2] K. Finkenzeller, *RFID Handbook*, 3rd ed. Hoboken, NJ, USA: John Wiley & Sons, 2010.

[3] S. Preradovic, I. Balbin, N. C. Karmakar, and G. F. Swiegers, "Multiresonator-based chipless RFID systemfor low-cost item tracking," *IEEE Trans. Microw. Theory Tech.*, vol. 57, no. 5, pp. 1411–1419, May 2009.

[4] D. Dardari and R. D'Errico, "Passive ultrawide bandwidth RFID," in *Proc. IEEE Global Telecommun. Conf. (GLOBECOM)*, 2008, pp. 1–6.

[5] S. Hu, Y. Zhou, C. L. Law, and W. Dou, "Study of a uniplanar monopole antenna for passive chipless UWB-RFID localization system," *IEEE Trans. Antennas Propag.*, vol. 58, no. 2, pp. 271–278, Feb. 2010.

[6] A. Ramos, A. Lázaro, D. Girbau, and R. Villarino, "Time-domain measurement of time-coded UWB chipless RFID tags," *Progress Electromagnetics Res.—PIER*, vol. 116, pp. 313–331, 2011.

[7] A. Lazaro, A. Ramos, D. Girbau, and R. Villarino, "Chipless UWB RFID tag detection using continuous wavelet transform," *IEEE Antennas Wireless Propag. Lett.*, vol. 10, pp. 520–523, 2011.

[8] S. Preradovic, N. Karmakar, and M. Zenere, "UWB chipless tag RFID reader design," in *Proc. IEEE Int. Conf. RFID-Technol. Appl.* , Guangzhou, China, June 17–19, 2010.

[9] A. Lazaro, D. Girbau, and D. Salinas, "Radio link budgets for UHF RFID on multipath environments," *IEEE Trans. Antennas Propag.*, vol. 57, no. 4, pp. 1241–1251, Apr. 2009.

[10] A. Lazaro, D. Girbau, and R. Villarino, "Effects of interferences in UHF RFID systems," *Progress Electromagn. Res.—PIER*, vol. 98, pp. 425–443, 2009.

[11] J. Lorenzo, D. Girbau, A. Lázaro, and R. Villarino, "Read range reduction in UHF RFID due to antenna detuning and gain penalty," *Microw. Opt. Technol. Lett.*, vol. 53, no. 1, pp. 144–148, 2011.

[12] B. A. Munk, *Frequency Selective Surfaces*. New York, NY, USA: Wiley, 2000.

[13] B. A. Munk, R. G. Kouyoumjian, and L. Peters, "Reflection properties of periodic surfaces of loaded dipoles," *IEEE Trans. Antennas Propag.*, vol. AP-19, no. 5, pp. 612–617, Sep. 1971.

[14] P. S. Neelakanta, A. K. Stampalia, and D. De Groff, "An actively-controlled microwave reflecting surface with binary-pattern modulation," *Microw. J.*, vol. 46, no. 12, pp. 22–35, Dec. 2003.

[15] G. Marrocco, "RFID grids: Part I—Electromagnetic theory," *IEEE Trans. Antennas Propag.*, vol. 59, no. 3, pp. 1019–1026, Mar. 2011.

[16] M. Ghavami, L. B. Michael, and R. Kohno, *Ultra Wideband Signals and Systems in Communication Engineering*. Hoboken, NJ, USA: Wiley, 2004.

[17] ***[AU: Please provide more information.]*** [Online]. Available: http://www.novelda.no/content/radar-icsNovelda AS, Garverivegen 2,NO-3850 Kviteseid, Norway, Website:

[18] J. Ansari, D. Pankin, and P. Mähönen, "Radio-triggered wake-ups with addressing capabilities for extremely low power sensor network applications," *Int. J. Wireless Inf. Netw.*, vol. 16, pp. 118–130, 2009.
[19] G. Vannucci, A. Bletsas, and D. leigh, "A software. defined radio system for backscatter sensor networks," *IEEE Trans. Wireless Commun.*, vol. 7, no. 6, pp. 2170–2179, Jun. 2008.
[20] A. Ferrer-Vidal, A. Rida, S. Basat, L. Yang, and M. M. Tenzeris, "Intergration of sensors and RFID's on ultra-low-cost paper-based substrates for wirelss sensor networks applications," presented at the 2006 2nd Workshop Wireless Mesh Netw. (WiMesh 2006), .
[21] R. E. Collin and F. J. Zucker, *The Receiving Antenna, Antenna Theory*. New-York, NY, USA: McGraw-Hill, 1969, part 1.
[22] R. B. Green, The General Theory of Antenna Scattering ElectroScience Laboratory Columbus, OH, USA, Tech. Rep. 1223-17, 1963.
[23] P. V. Nikitin, K. V. S. Rao, S. F. Lam, V. Pillai, R. Martinez, and H. Heinrich, "Power reflection coefficient analysis for complex impedances in RFID tag design," *IEEE Trans. Microw. Theory Tech.*, vol. 53, no. 9, pp. 2721–2725, Sep. 2005.
[24] S. Licul and W. A. Davis, "Unified frequency and time-domain antenna modeling and characterization," *IEEE Trans. Antennas Propag.*, vol. 53, no. 9, pp. 2882–2888, Sep. 2005.
[25] Y. Duroc, T.-P. Vuong, and S. Tedjini, "A time/frequency model of ultrawideband antennas," *IEEE Trans. Antennas Propag.*, vol. 55, no. 8, pp. 2342–2350, Aug. 2007.
[26] ***[AU: Please provide more info.]*** [Online]. Available: http://www.microchip.com/wwwproducts/Devices.aspx?dDocName=en538963#1PIC16(L)F1826/27 18/20/28-Pin Flash MCU with nanoWatt XLP, 2011 Microchip Technology Inc. Available in:
[27] ***[AU: Please provide more info.]*** Application Note AN 1089 Designing Detectors for RF ID Tags, Avago Technologies.
[28] M. N. Jazi and T. A. Denidni, "Frequency selective surfaces and their applications for nimble-radiation pattern antennas," *IEEE Trans. Antennas Propag.*, vol. 58, no. 7, pp. 2227–2237, Jul. 2010.
[29] ***[AU: Please provide more info.]*** 2004, BAP51-03. General purpose PIN diode, NXP.
[30] Application Note 1330, HMPP-3865 MiniPAK PIN Diode High Isolation SPDT Switch Design for 1.9 GHz and 2.45 GHz Applications, Avago Technologies.
[31] H. A. Hjortland, D. T. Wisland, T. S. Lande, C. Limbodal, and K. Meisal, "Thresholded samplers for UWB impulse radar," in *Proc. IEEE Int. Symp. Circuits Syst. (ISCAS 2007)*, New Orleans, LA, USA, May 27–30, 2007, pp. 1210–1213.
[32] A. Lazaro, D. Girbau, and R. Villarino, "Weighted centroid method for breast tumor localization using an UWB RADAR," *Progress Electromagn. Res. B*, vol. 24, pp. 1–15, 2010.
[33] A. Mehdipour, K. Mohammadpour-Aghdam, and R. Faraji-Dana, "Complete dispersion analysis of Vivaldi antenna for ultra wideband applications," *Progress Electromagn. Res., PIER 77*, pp. 85–96, 2007.

Antonio Lázaro (M'07) was born in Lleida, Spain, in 1971. He received the M.S. and Ph.D. degrees in telecommunication engineering from the Universitat Politècnica de Catalunya (UPC), Barcelona, Spain, in 1994 and 1998, respectively.

He then joined the faculty of UPC, where he currently teaches a course on microwave circuits and antennas. In July 2004. he joined the Department of Electronic Engineering, Universitat Rovira i Virgili, Tarragona, Spain. His research interests are microwave device modeling, on-wafer noise measurements, monolithic microwave integrated circuits (MMICs), low phase noise oscillators, MEMS, and microwave systems.

Angel Ramos received the B.S. degree in telecommunication engineering and the M.S. degree in electronic engineering from Universitat Rovira i Virgili (URV), Tarragona, Spain, in 2010 and 2011, respectively. He is currently working toward the Ph.D. degree within the Department of Electronics, Electrics and Automatics Engineering at URV.

David Girbau (M'04) received the B.S. degree in telecommunication engineering, the M.S. degree in electronics engineering, and the Ph.D.degree in telecommunication from Universitat Politècnica de Catalunya (UPC), Barcelona, Spain, in 1998, 2002, and 2006, respectively.

From February 2001 to September 2007, he was a Research Assistant with the UPC. From September 2005 to September 2007, he was a Part-Time Assistant Professor with the Universitat Autònoma de Barcelona (UAB). Since October 2007, he has been a Full-Time Professor at Universitat Rovira i Virgili (URV). His research interests include microwave devices and systems, with emphasis on UWB, RFIDs, and RF-MEMS.

Ramon Villarino received the B.Sc. degree in telecommunications eechnical engineering from the Ramon Llull University (URL), Barcelona, Spain, in 1994, the M.Sc. degree in senior telecommunications engineering from the Polytechnic University of Catalonia (UPC), Barcelona, Spain, in 2000, and the Ph.D.degree from the UPC, in 2004.

During 2005–2006, he was a Research Associate at the Technological Telecommunications Center of Catalonia (CTTC), Barcelona, Spain. He worked at the Autonomous University of Catalonia (UAB) from 2006 to 2008 as a Researcher and Assistant Professor. Since January 2009, he has been a Full-Time Professor at Universitat Rovira i Virgili (URV). His research interests include radiometry, microwave devices, and systems, based on UWB, RFIDs, and frequency selective structures using MetaMaterials (MM).

A Novel UWB RFID Tag Using Active Frequency Selective Surface

A. Lazaro, *Member, IEEE*, A. Ramos, D. Girbau, *Member, IEEE*, and R. Villarino

***Abstract*—This work describes an actively controlled frequency selective surface (FSS) to implement ultrawideband radio identification (RFID) tags. The tag exploits the change in the radar cross section (RCS) of the FSS, which is loaded with switching PIN diodes to modulate the backscattered time-domain response of the tag to an input ultra-wide band pulse. The basic operation theory of the system is explained. An experimental setup based on a ultrawideband radar working as a reader is proposed to measure the modulated radar cross section of the tags. As a proof of concept, a battery-assisted or semipassive tag has been developed.**

***Index Terms*—Frequency selective surface (FSS), radio frequency identification (RFID), ultrawideband UWB, wake-up circuit.**

I. Introduction

ULTRAWIDEBAND (UWB) technology has been recently allowed for its commercial operation in communications. Thus, the use of UWB technology has changed dramatically in recent years [1]. In this context, UWB technology is also a promising solution for next generation radiofrequency identification (RFID) systems to overcome some of the limitations of the current narrow-band RFID technology [2], and it is also an enabling technology for future wireless sensors. UWB chipless tags for RFID systems might be a good alternative for low-cost item tagging, as recently demonstrated in [3]–[8]. Printable chipless RFID tags based on multiresonators have been reported in [3], [8], where the information is coded in frequency domain. An alternative method where the information is coded in the time delay has been proposed in [4]–[7]. However, the number of bits that chipless tags can code is small for some applications, and chip-based tags are needed. Chip-based RFID tags must receive DC power to be read. This power can come either from a battery or from the reader's signal, which is rectified to overcome a threshold voltage. The nonbattery powered chip-based tags are referred to as passive. These have a limited dynamic range determined by the regulatory limits of broadcast power and by the forward loss of signal that falls below the threshold required. In semipassive tags, battery power can be supplied to the IC in order to overcome the forward loss. Finally, active tags also use the battery power to generate and send the return signal [2].

Passive RFID tags are based on backscatter modulation, where the antenna reflection properties are changed according to the code stored in the tag. Although several frequency bands exist as a function of the application, UHF passive tags are preferred due to the compromise between price, memory capacity and distance. HF and MF frequency tags are reserved for short distances (they are based in magnetic coupling, which decreases much faster than the far field coupling used in UHF or microwave tags). However, UHF RFID technology has some drawbacks. The frequency band allocation for UHF RFID depends on the country and the read range is limited by the power transmitted from the reader, a parameter which is not the same all over the world. The read range is influenced by multipath propagation [9] and interference between readers [10]. In addition, UHF tags suffer from frequency detuning when they are attached to materials [9], [11]. Furthermore, special tags must be used in presence of metals or liquids, increasing the tag price.

Controllable electromagnetic absorption and/or reflection by materials is an important issue in the development of radar absorbing surfaces and in certain EMI/EMC problems. Conventionally, microwave materials composed by a combination of metallic and/or nonmetallic (dielectric) absorbing constituents are used for this purpose [12], [13]. The concept of facilitating such modulating capability in an electromagnetic reflecting surface is also useful in designing RFID tags [14], [15]. In this paper, the backscattering approach is based on the modulation of active controlled reflecting surface. Basically, the radar cross section (RCS) depends on the surface shape, area and materials. For instance, Fig. 1 shows a frequency selective surface (FSS) which is made by a two-dimensional array of dipoles, which in turn are loaded with switching diodes [13]. Thus, when the diodes are unbiased, they present a high-impedance state and the electromagnetic wave passes through the surface. Under these load conditions, the FSS is like an array of dipoles with half-length with respect the forward-biased case. In this case the surface presents a low RCS state (see the equivalent circuit of an FSS and the approximated current distribution shown in Fig. 2). But, when they are biased on, the diodes present a low-impedance state and the surface is like an array of rods that acts as a polarized grid, reflecting the electromagnetic waves. In this second case, the surface presents a high RCS state. Switching the diodes state, the electrical lengths of the dipoles change, resulting in modulation of the resonance frequency of the FSS. A large difference in the RCS is expected depending on the state of the diodes. Then the tag works as follows [see Fig. 3(a)]:

Manuscript received January 25, 2012; revised September 12, 2012; accepted November 09, 2012. Date of publication November 21, 2012; date of current version nulldate. This work was supported by the Spanish Government Project TEC2011-28357-C02-01.

The authors are with the Electronics, Electrical, and Automatics Engineering Department, Universitat Rovira i Virgili, 43007 Tarragona, Spain (e-mail: antonioramon.lazaro@urv.cat; angel.ramos@estudiants.urv.cat; david.girbau@urv.cat; ramon.villarino@urv.cat).

Color versions of one or more of the figures in this paper are available online at http://ieeexplore.ieee.org.

Digital Object Identifier 10.1109/TAP.2012.2228838

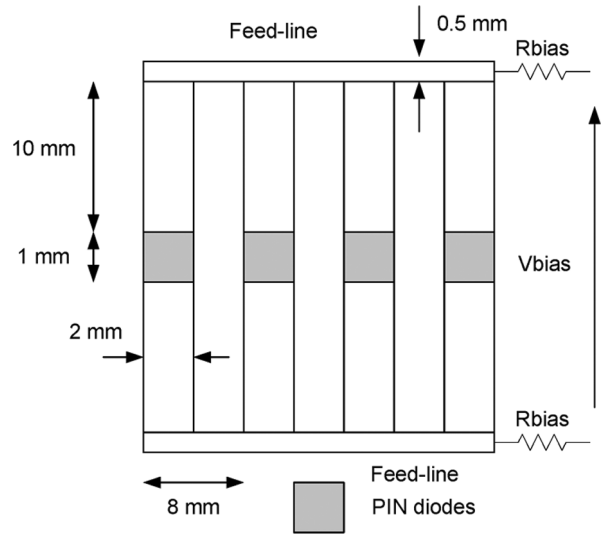

Fig. 1. Diagram of a FSS used in time-domain UWB tag including the dimensions of the manufactured FSS.

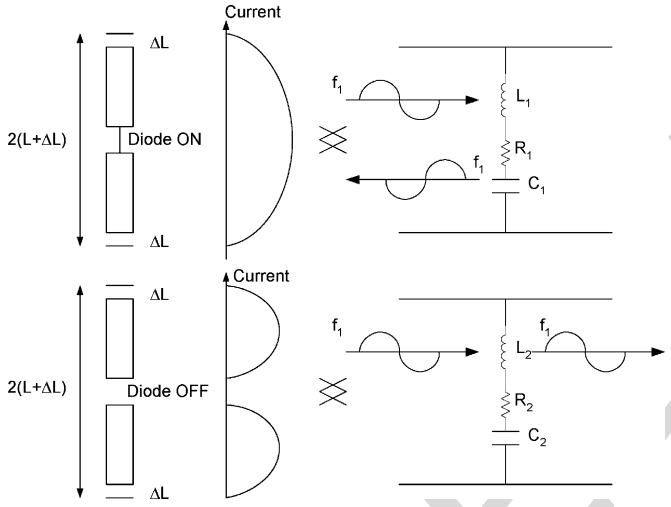

Fig. 2. Equivalent circuit model of the FSS for the two diode states. When the diode is shorted (diode ON), the waves with frequencies near the resonance frequency (f_1) are reflected, whereas the FSS is transparent for these waves when the diode is open-circuit (Diode OFF).

the reader illuminates the tag with an electromagnetic wave and part of the power is reflected due to its RCS. The information is coded in the change of the RCS due to the active elements printed on the surface of the tag.

The active reflecting surface has been used to modulate the RCS of a narrowband signal as described in [14] and [15]. But, it can also be used to modulate the amplitude of a short-time UWB pulse. This last approach is proposed in this paper. As a consequence the time-of-flight between the transmitted pulse and the modulated received pulse can be measured, permitting the localization of the tag. This feature is particularly interesting as a simple anticollision technique in dense tag scenarios, because the collected tags response can be filtered as function of the distance or its equivalent time delay. Using the UWB band allows to solve typical UHF RFID problems explained before. UWB antennas have already been used for RFID applications

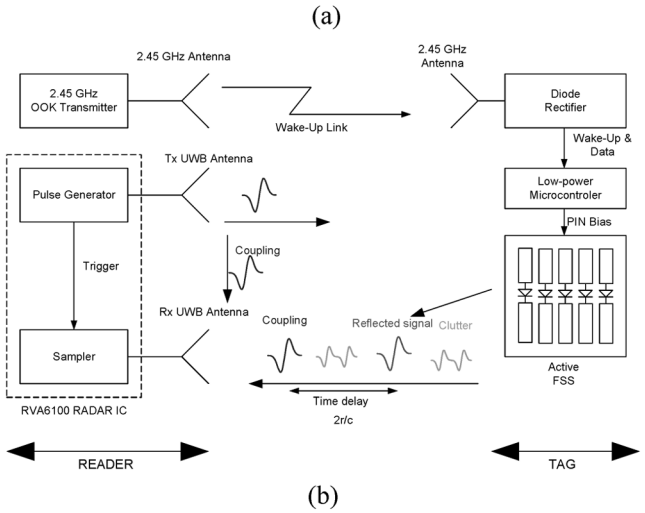

Fig. 3. (a) Block diagram schema and photograph (b) of the experimental RFID system based on a UWB radar and an FSS UWB RFID tag.

in time-domain. One approach is to code the information in the delay such as in passive chipless time-domain UWB tags [7]. Another approach consists on modulating the amplitude of the backscattering antenna mode, by changing the load impedance [5]. In this work, it is proposed to replace the UWB antenna by an active FSS. Although the communication between the tag and the reader is also done by backscattering (by modulating the load of the FSS), some important differences should be pointed out. First, the tag is illuminated by a wideband signal (UWB short pulse with wideband spectrum) instead of a CW signal. In consequence, the backscattered field on the entire pulse spectrum should be taken into account. Since FSSs are frequency-selective circuits, the reflected pulse will suffer some type of distortion. However, as it will be discussed later, it is possible to detect this pulse using standard UWB detection schemes based on matched filters or even based on energy or peak detectors [16]. For instance, in a matched filter detector, the output of the detector is proportional to the energy of the reflected pulse. Then, the key in this work is that the energy of the reflected pulse is modulated due the change in the backscattering field (and RCS) of the FSS. The FSS can be viewed as a tunable filter that filters the spectrum of the incident wideband pulse, changing the energy and also the amplitude of the reflected pulse in time domain. Second, since the RCS of an FSS increases with the number of elements, using an FSS instead of a UWB antenna can help to improve the detection of the tag. In addition, the experimental results show that it is possible to implement a low-cost UWB RFID reader using commercial UWB radars

instead of expensive instruments such as vector network analyzers or wideband oscilloscopes. In this work, an integrated UWB low-power radar from Novelda Norway [17] is used as the low-cost reader.

The paper is organized as follows. Section II deals with the basic theory of time-domain UWB RFID with active controlled FSS. Section III describes the semipassive or battery-assisted tag designed as proof of concept. The design of the active reflecting surface is given based on electromagnetic simulations. In addition, the idea of using a second radio signal to wake up the tag IC is used. Compared with previous wake-up circuits presented in the literature [18]–[20], the wake-up circuit saves power consumption because it uses the internal microcontroller comparator without the need for adding additional operational amplifiers or comparators. Section IV describes the experimental results obtained with the system. Section V draws the conclusions.

II. FSS as a UWB RFID Tag

A. Scattering Fields.

The proposed system is shown in Fig. 3. It consists of a bistatic IR-UWB radar that illuminates the tag. When the transmitted pulse hits the tag antenna, a portion of the pulse is backscattered towards the receiver. The tag consists of a FSS loaded with PIN diodes that modulate the backscattered field of the tag. In this work, an array of dipoles is considered as the FSS. Then, an active FSS can be viewed as an array of antennas loaded with the impedance of the PIN diodes. Thus, the backscattered field can be studied using fundamental antenna scattering theory [21], [22].

The backscattered field of an antenna can be split as a sum of two terms: a structural mode and an antenna mode, or a load-independent term and a load-dependent term, respectively

$$\overline{E}_s(Z_L) = \overline{E}_s(Z_{\text{ref}}) - \left(I_{\text{ref}}\overline{E}_r\right)\Gamma \tag{1}$$

where $E_S(Z_L)$ is the scattered field by the tag connected to the load Z_L, $E_S(Z_{\text{ref}})$ is the scattered field when the tag is connected to a reference load Z_{ref}, I_{ref} is the current of the antenna when connected to a load Z_{ref} and E_r is the radiated field of the antenna as a receiving antenna under a unit current source.

Depending on the author, the reference impedance can change, but often following the Green's work [22], $Z_{\text{ref}} = Z_a^*$, where Z_a is the antenna's impedance. Γ is the power reflection coefficient given by: $\Gamma = (Z_L - Z_a^*)/(Z_L + Z_a)$.

Then, the antenna reflects the structural mode when the load is the conjugate impedance of the antenna impedance. In this case, all the incident power is transferred to the load and the antenna only reflects the structural mode. The structural mode arises from the induced current on the antenna conducting surface by the incident wave, and it does not depend on the load. The structural mode depends on characteristics such as the antenna type, geometry, and material. Thus, the structural mode is independent of the load reflection coefficient, whereas the antenna mode is proportional to it.

The radar cross-section of a target is a far-field quantity that can be expressed by using (1) as

$$\text{RCS} = \left|\sqrt{\text{RCS}_{\text{struc}}} + \sqrt{\text{RCS}_a}e^{j\varphi_{as}}\right|^2 \tag{2}$$

where $\text{RCS}_{\text{struc}}$ is the RCS due to structural mode, RCS_a is the RCS due to antenna mode (which depends on the load), and ϕ_{as} is the phase difference between these two modes.

In conventional narrowband RFID systems the incident continuous wave (CW) at the tag antenna is modulated by changing the tag's load between two values. The received power for each state is proportional to the RCS given by (2). In passive RFID systems, the mean power between the two states should be greater than a minimum threshold power in order to obtain the enough DC power for the chip operation. As most RFID readers use coherent receivers, the bit error rate (BER) is a function of the difference between the backscattered fields for the two states. In consequence, the BER is optimized by maximizing the differential RCS, as defined by [23]

$$\text{RCS}_{\text{dif}} = \frac{\lambda^2}{4\pi}G^2|\Gamma_{\text{on}} - \Gamma_{\text{off}}|^2 = \frac{4\pi}{\lambda^2}A_{\text{ef}}^2|\Gamma_{\text{on}} - \Gamma_{\text{off}}|^2 \tag{3}$$

where A_{ef} is the effective area of the antenna, Γ_{on} and Γ_{off} are the reflection coefficients of the antenna load (i.e., chip) for each bit state, and λ is the wavelength. The structural component A_s is often omitted during the tag design process [23], claiming that this term does not influence the BER performance of the system, since it is common in the backscattered field, regardless of the connected load.

The RCS of a FSS depends on the frequency and its reflectivity. When the frequency of the incident wave is close to the dipoles resonance frequency (when the dipoles become approximately half wavelength [13]), the FSS presents a high reflectivity. This reflectivity is close to 1 at its resonant frequency. Thus, an important issue is that the RCS of an FSS of area A, near its resonance frequency, is proportional to the RCS of a flat plate (in optical region and with normal orientation) with the same area [12], [13].

Considering an FSS as an array of antennas, it can potentially be used to improve the detection of tags in traditional narrowband backscattering RFID systems. If the distance between the elements of the FSS is small compared to the operating wavelength, the gain is approximately equal to the gain of one single element multiplied by the number of elements in the FSS (assuming there is not a polarization mismatch and the FSS is oriented to the reader). This fact is also used in grid arrays of tags proposed in [15] to improve the reading range and tag gain.

B. Tag Detection

In order to design a UWB tag based on an FSS it is important to understand the interaction between the radar and the tag in time domain. In the case of a free-space channel and assuming a monostatic reader, the received signal is written in the frequency domain as

$$S(\omega) = H_{\text{TX}}(\omega)H_{\text{CH}}(\omega, r)\frac{\sqrt{\text{RCS}}e^{j\phi}}{\lambda} \times H_{\text{CH}}(\omega, r)H_{\text{RX}}(\omega)P(\omega) \tag{4}$$

where ϕ is the phase of the backscattered signal, ω is the angular frequency, $P(\omega)$ is the Fourier transform of the transmitted pulse and the free-space channel transfer function $H_{\rm CH}$ is given by [24], [25]. In practice, the channel transfer function $H_{\rm CH}$ in (4) can be characterized from the measured S_{21} parameter as a function of the frequency using a Vector Network Analyzer (the TX antenna is connected to port 1, and the RX one to port 2). Moreover, the product $H_{\rm TX}(\omega)H_{\rm CH}(\omega)H_{\rm RX}(\omega)$ can be obtained from the Fourier transform of the received time domain signal $(s_{\rm cal}({\rm t}))$ measured by the radar receiver when the TX and RX antennas are oriented face-to-face and spaced a distance $r_{\rm cal}$

$$S_{\rm cal}(\omega) = \Im(s_{\rm cal}(t)) = H_{\rm TX}(\omega)H_{\rm CH}(\omega, r_{\rm cal}) \times H_{\rm RX}(\omega)P(\omega). \quad (5)$$

Then, the received signal as function of the frequency can be written as

$$S(\omega) = S_{\rm cal}(\omega)\frac{r_{\rm cal}}{r}e^{-jk(r-r_{\rm cal})}H_{\rm CH}(\omega, r)\frac{\sqrt{\rm RCS}e^{j\phi}}{\lambda}. \quad (6)$$

Finally, the received signal in time domain $(s(t))$ can be obtained from the Inverse Fourier transform of $S(\omega)$.

From the previous discussion it is expected an important difference in the level of the reflected signal by the FSS as a function of the load impedance. It can be observed that the amplitude of the received signal when the FSS is loaded with an open-circuit (diodes OFF) is much lower than when the FSS is loaded with a short-circuit (diodes ON). This makes possible to use the FSS to modulate the amplitude of UWB pulses. Unfortunately, the difference in the RCS between the ON and OFF diodes states is smaller than in the ideal case, mainly due to the effect of diode parasitic elements, as it will be studied in Section III.

Common UWB detection methods can be used to demodulate the received pulse $s(t)$. The most simple is a peak detector. Since the amplitude of the received pulse is a function of the backscattering field at each state of the FSS, a threshold comparator can be used to demodulate the signal. Other common technique is using a matched filter or a correlator. In this approach, the received signal is correlated with a stored template. The output of this detector is proportional to the energy of the received pulse. This energy can be computed by using the Parseval's theorem and (4)

$$E = \int_{-\infty}^{+\infty}|s(t)|^2dt = \frac{1}{2\pi}\int_{-\infty}^{+\infty}|S(\omega)|^2d\omega. \quad (7)$$

It can be noted that the energy does not depend on the phase ϕ of the backscattered signal. The peak detector and the matched filter methods, however, have some problems. The mached filter maximizes the signal to noise ratio in the sampling instant if the template signal is the same (or proportional) to the received pulse. In practice, the shape of the received pulse due to the distortion introduced by the reader's Tx and Rx antennas, as well as the FSS frequency response, may be difficult to know *a priori*. A solution to this problem may be to use the technique proposed by the authors in [7] using a Wavelet decomposition as a bank of matched filters. Another issue in both detectors is the need to remove the received pulses due to multipath components caused by reflections in objects near the tag. This can be done by substracting a previously stored signal without the presence of the tag, called background subtraction. This calibration can be easily done if the environment is stationary and the surrounding objects do not change their position around the tag with the time. Unfortunately, this is not the real case, since an RFID reader can move its position, which requires a periodic calibration. To solve this problem, a differential approach is proposed in this work. The information can be coded in the change of states. The differential signal considered is the substraction between each signal and a previously stored received signal (which can be the signal corresponding to the first bit of a short sequence, or the signal corresponding to the immediately previous bit). The background and clutter multipath components will be removed, since they will be the same for both states. This assumption is reasonably certain if high or moderate transmission rates are used, because the reference signal has very similar background and clutter components. The differential signal is proportional to the difference between two backscattering fields and it can be obtained calculating the difference for the two states using (6). Similar to narrow band RFID systems, this difference can be expressed as function of the differential RCS

$$S_{\rm dif}(\omega) = \Delta S(\omega) = S_{\rm cal}(\omega)\frac{r_{\rm cal}}{r}e^{-jk(r-r_{\rm cal})} \times H_{\rm CH}(\omega, r)\frac{\sqrt{\rm RCS_{dif}}}{\lambda}. \quad (8)$$

Again (8) does not depend neither on phase ϕ or on the structural mode. These differential schemas are compatible with mached filter (or Wavelet detection) approaches because the template is a previously received signal. However, as it will be shown in the results, a simple envelope detector with a comparator can be used instead of these approaches.

III. Tag Design

As a proof of concept, a semipassive tag has been designed (see Fig. 4). The tag is composed by the following blocks [as shown in Fig. 3(a))]: a diode rectifier (to obtain a 2.4 GHz tone wakeup signal from the reader), a low power microcontroller, and an active FSS. Recently, ultra-low power microcontrollers have been commercialized by Microchip. The PIC 16F1827 [26] is selected for this design. It consumes less than 100 nA in sleep mode, and 210 μA at a 1 MHz clock. The tag is powered by a 3 V Lithium battery. In wireless sensor networks, the tag is normally inactive for long time periods [18]. During these time intervals the microcontroller rests in sleep mode (low-power consumption state), and it only wakes up when it receives a wakeup signal from the reader or periodically to acquire a sensor measurement. The life of the battery depends on the time the receiver and transmitter are active.

A. Wake-Up Circuit

Wakeup radio avoids the complex bookkeeping associated with energy-efficient MAC protocols, but at the price of additional hardware [18]–[20]. So that a receiver can fire up its

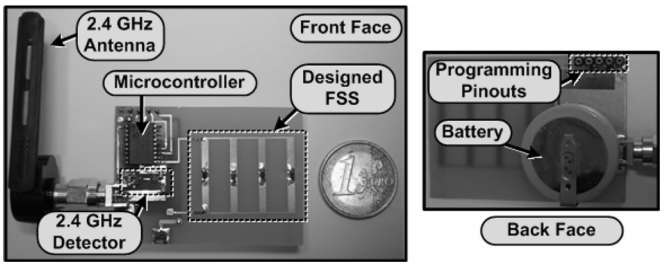

Fig. 4. Photograph of the designed tag, front (left) and back (right).

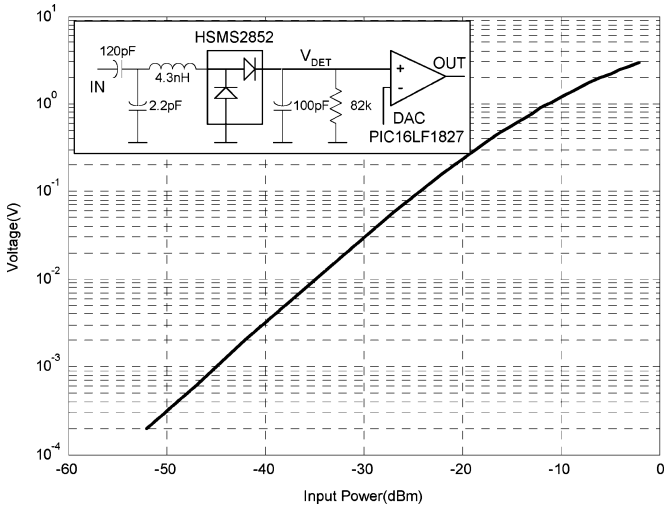

Fig. 5. Wake-up and data demodulator based on a Schottky diode detector and measured voltage detected for the designed detector.

primary radio to engage in efficient high-speed communication with the sender. In our case, a 2.45 GHz Schottky diode-based detector is used as the receiver. The reader sends an on-off-keying (OOK) modulated signal to wake up the tag. In order to prevent random wake up due to in-band interference from other systems, the tag only wakes up when a previously known stored bit sequence is received. This sequence can be considered as an address to select a specific tag or sensor within a wireless sensor network. The diode detector schema is shown in Fig. 5. It is composed by a LC matching network tuned at 2.45 GHz and two zero bias diodes in series configuration (Avago HSMS-2852) [27]. The output of the diodes is filtered by a parallel RC network and it is directly connected to an internal comparator of the microcontroller. The voltage threshold of the comparator is configurable via the internal digital-to-analog converter (DAC) of the microcontroller. This fact allows a tunable minimum wake-up distance without adding additional components to the tag, saving power consumption and protecting from unintended wake ups. When this threshold is exceeded by the rectified signal, the microcontroller executes an interrupt routine. Then, it sends the stored data (an identification code) by changing the voltage of the PIN diodes that load the FSS. After this process, the microcontroller returns to sleep mode to increase the battery life time.

The maximum read range obtained with this demonstrator is about 2 meters, thus the 2.45 GHz ISM band allows an EIRP up to 27 dBm (for outdoor mode in Europe). If a higher wake-up

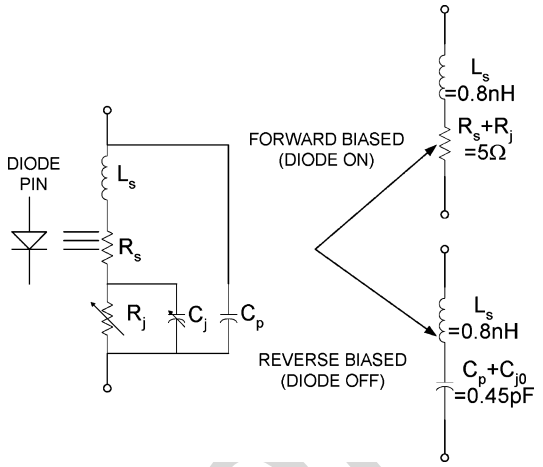

Fig. 6. High frequency equivalent circuit for the PIN diode used.

distance is required, the UHF RFID band can be used, since a higher maximum transmitted power is available (0.5 W under ETSEI EN 300 220 or 2 W under ETSI EN 302 208, and 4 W under FCC in US). The band change can be done with a simple modification of the tuned LC matching circuit. Fig. 5 shows the measured detected voltage ($\mathrm{V_{DET}}$) as a function of the power level for an input tone at 2.45 GHz. The detector sensitivity is adjusted to about -40 dBm by setting the threshold voltage to 3 mV in the comparator using the DAC. This sensitivity corresponds to a distance higher than 10 m using a dual-polarized patch antenna which transmits a 20 dBm EIRP, and a dipole antenna in the tag. Thus, the read range in our demonstrator is limited by the UWB down-link rather than the 2.45 GHz wake-up link.

B. FSS Design

The FSS is designed using a low-cost 1.6 mm thick FR4-Epoxy substrate (relative permittivity $\varepsilon_{\mathrm{r}} = 4.4$, loss tangent $\tan\delta = 0.02$). High frequency PIN diodes are one of the most commonly used active elements applied to reconfigure the EM response of a FSS surface [12], [13], [28]. Fig. 6 depicts the applied electrical circuit model of the BAP51-03 PIN-Diode [29] in the simulation [29], [30] for the two-states. In the forward biased case, the diode mainly represents a small resistance, which has small effect on the desired response of the FSS surface. Because of its small value, the series self inductance of the diode in this case should be considered for simulations in UWB. However, when it is reverse biased, the parasitic capacitance considerably deviates the position of the surface stop-band by altering the total effective capacitance of the unit cell. Therefore, it is required to consider its effect in the design process.

The length of the dipoles is chosen to resonate at the peak frequency of the transmitted UWB pulse (about 4 GHz) when the diodes are forward biased (approximately loaded with a short circuit). When the diodes are reverse biased, their impedance is approximately equal to the parasitic capacitance C_p plus a junction capacitance C_{j0} ($C_p + C_{j0} = 0.45$ pF), in series with a 0.8 nH parasitic inductance L_s. Thus, an important shift in the resonance frequency of the FSS is expected in the reverse biased state. It is not trivial to compute the exact circuit parameters of

the FSS, and in practice a numerical approach is necessary [12], so FEKO using Multilevel Fast Multipole Method (MLFMM) has been used to carry out the numerical simulations. The diodes are modeled using lumped elements such as the ones shown in Fig. 6. The dimensions of the FSS designed are shown in Fig. 1. The FSS is composed by four printed dipoles with 20 mm length and 2 mm width. The feed lines width is 0.5 mm, and the spacing between the dipoles is 8 mm. The diodes are biased using high impedance transmission lines connected to the bias resistor to limit the current. The feed lines are connected at the end of the dipoles, presenting a high impedance in order to not change the current distribution, in constrast with an ideal dipole which presents an open circuit at these points. To avoid increasing the number of resistors, the bias resistors are connected at the end of the feed lines (see *Rbias* in Fig. 1). As the impedance associated to the parasitic inductance dominates over the diode resistance and to limit the power consumption, the diodes are biased at 0.5 mA in forward conditions ($\mathrm{V_{bias}} = 3$ V, $\mathrm{R_{bias}} = 2.3$ kΩ).

Fig. 7 shows the RCS of the FSS for different load conditions. This figure compares the RCS for the FSS loaded with an ideal short-circuit ($Z_L = 0$), an ideal open-circuit ($Z_L = \infty$), when the PIN diodes biased on ($I = 0.5$ mA, $Z_L = j\omega 0.8$ nH $+ 5$) and when it is in reverse bias ($\mathrm{V} = 0, Z_L = j\omega 0.8$ nH $+ 1/(j\omega 0.45$ pF$)$). A great difference in the RCS between short and open circuit load conditions is observed in the frequency band of the UWB radar (1–4.5 GHz). However, due to the diodes parasitic capacitance, the shift in the FSS resonant frequency is reduced. The difference between the RCS states is also reduced. In order to investigate the effect of the feed lines, Fig. 8 shows the simulation for the same load conditions of four dipoles without the feed lines. We observe a change in the shape of the resonance. But in the frequency range of interest the change is not very significant for our purposes. In both cases, the bandwidth of the resonance is higher than in free space as an effect of the dielectric thickness [12]. Fig. 9 shows the simulated RCS for a single printed dipole. The dimensions of the dipole are the same than the ones for a dipole element in the FSS of Figs. 7–8. It can be observed that the bandwidth of the FSS is larger than the dipole antenna. The peak of the RCS at the resonant frequency in the case of the FSS is higher than in the case of the dipole antenna. Figs. 10–12 show the phase of the backscattered field of the tag including the feed lines, without the feed lines and with a printed dipole antenna, respectively. In all the cases, at low frequency the phase is close to 180°. In this frequency range, the FSS acts as a metallic reflector because the separation between the rods is small compared with the wavelength. The phase decreases faster when the frequency is close to the resonant frequency of the dipoles. According to the equivalent circuits of Fig. 2., the resonant frequency of a FSS loaded with an open circuit is about the double than when it is loaded with a short circuit. So, important differences in the backscattering phase can be shown between open and short circuit load conditions. Due to the parasitic effect of PIN diodes, the change in the load impedance is not greater than between open and short circuit conditions, resulting in a similar backscattering phase behavior.

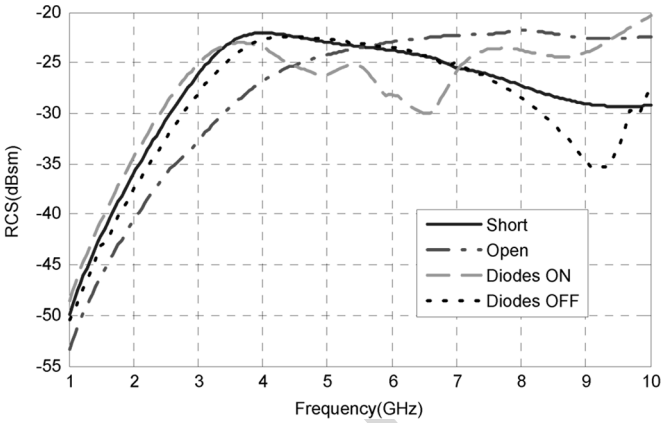

Fig. 7. Simulated RCS of the tag including feed lines.

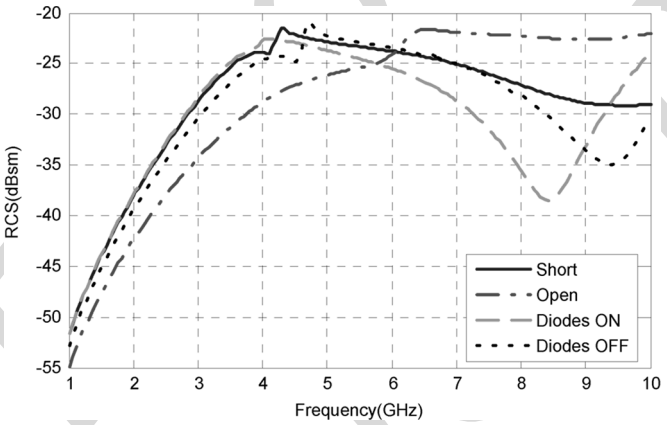

Fig. 8. Simulated RCS of the tag without the feed lines.

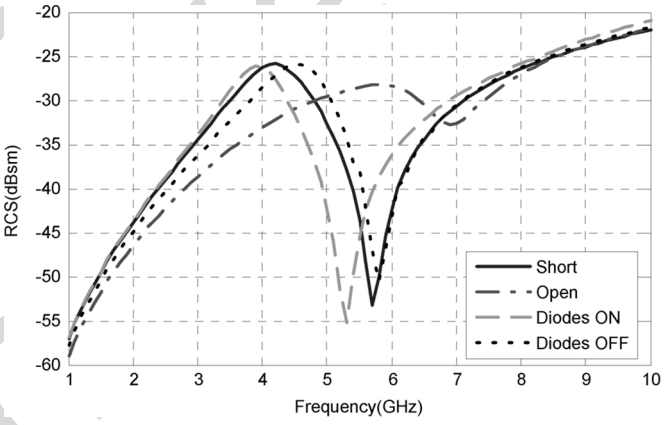

Fig. 9. Simulated RCS of a printed dipole.

From the last simulations the energy reflected by an FSS due its higher bandwidth will be higher than for a single dipole antenna. Also, the reflected pulses will suffer less distortion.

As explained before, if a differential detector is used, the received signal is a function of the differential RCS. From the scattering field given by (1) for short ($\Gamma = -1$) and open ($\Gamma = 1$) load conditions ($E_s(0)$ and $E_s(\infty)$, respectively), it is possible to separate the structural mode $E_S(Z_{\mathrm{ref}})$ and the antenna mode, which is proportional to $(I_{\mathrm{ref}} E_r)$

$$\overline{E}_s(Z_{\mathrm{ref}}) = (\overline{E}_s(0) + \overline{E}_s(\infty))/2 \tag{10}$$

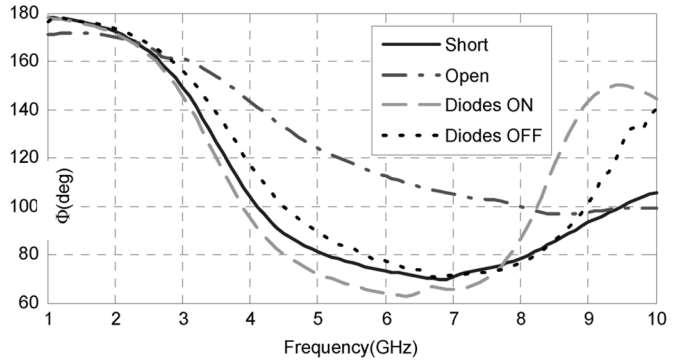

Fig. 10. Phase of the backscattered field of the tag including feeding lines.

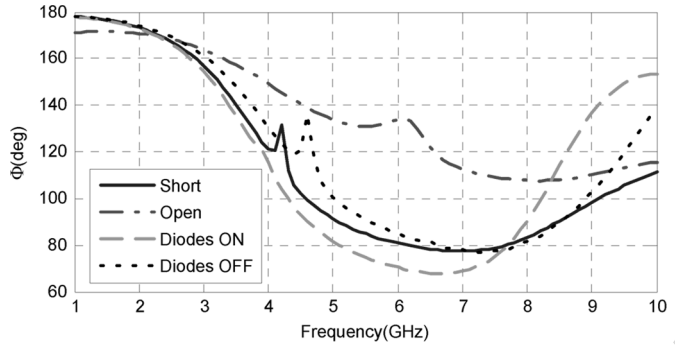

Fig. 11. Phase of the backscattered field of the tag without the feeding lines.

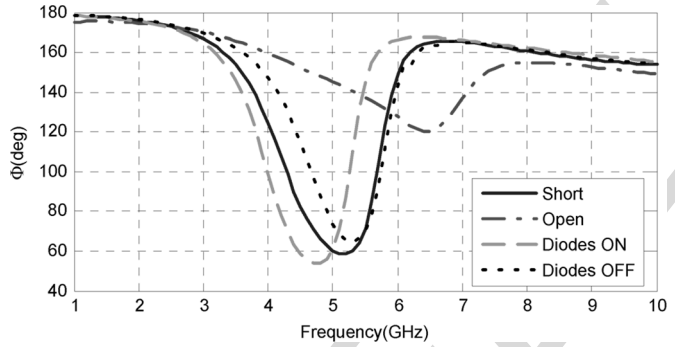

Fig. 12. Phase of the backscattered field of the printed dipole.

$$I_{\text{ref}}\overline{E}_r = (\overline{E}_s(0) - \overline{E}_s(\infty))/2. \qquad (11)$$

Fig. 13 investigates the frequency behavior of the structural and antenna modes for open and short load conditions (term $\mathrm{I_{ref}E}_r$) for the FSS designed. This figure compares the differential RCS obtained from the difference in the backscattering field for ideal short and open conditions and with the diodes in ON and OFF states. It can be observed that the structural mode for frequencies below the resonance is higher than the antenna mode. For frequencies greater than the resonance frequency, the antenna mode is the one that predominates. Depending on the phase of the load reflection coefficient, the sum can be constructive or destructive. So, the differential RCS between short and open load conditions is often higher than for other load conditions. Fig. 14 repeats the study for a printed dipole antenna. Finally, Fig. 15 compares the differential RCS for the FSS and the

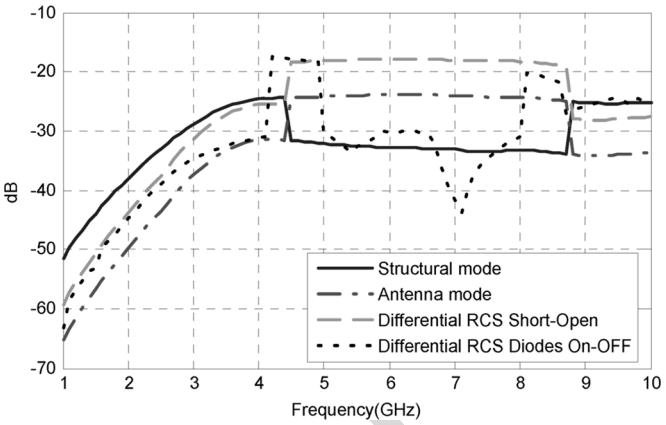

Fig. 13. FSS case: Structural mode and antenna mode for open condition, and differential RCS between Short-Open states and between Diodes ON-OFF states.

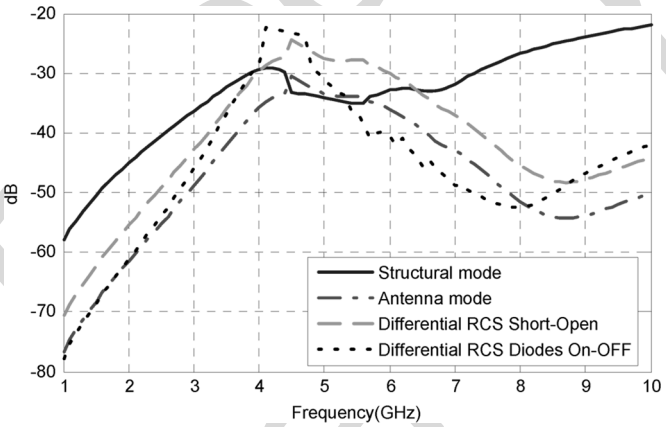

Fig. 14. Dipole case: Structural mode and antenna mode for open condition, and differential RCS between Short-Open states and between Diodes ON-OFF states.

printed dipole antenna. For the ideal short and open load conditions a considerable higher differential RCS in a large bandwidth is obtained. Using the PIN diodes, however, it is difficult to obtain such large difference between the two states. Thus, in the realistic case of the FSS and dipole antenna loaded with the PIN diodes, the bandwidth is reduced due the proximity between the reflection coefficients for the two states.

IV. Experimental Results

The experimental setup is shown in Fig. 3. The Novelda NVA6100 IC [17] is used as the reader. The NVA6100 is a fully-integrated nanoscale impulse radar transceiver, designed for low-power applications. Rather than continuously sampling the received signal, the NVA6100 employs a concept known as strobed sampling, which is described in [31]. For each pulse transmitted, the backscattered EM energy is sampled after a given time offset. This offset represents the time-of-flight of the signal relative to the time of transmission, which in turn can be used to represent the distance to the remote object. In order to avoid the Maximum Unambiguous Range limitation, a staggered pulse repetition frequency (PRF) has been used [31]. The radar generator transmits a near-Gaussian monocycle of

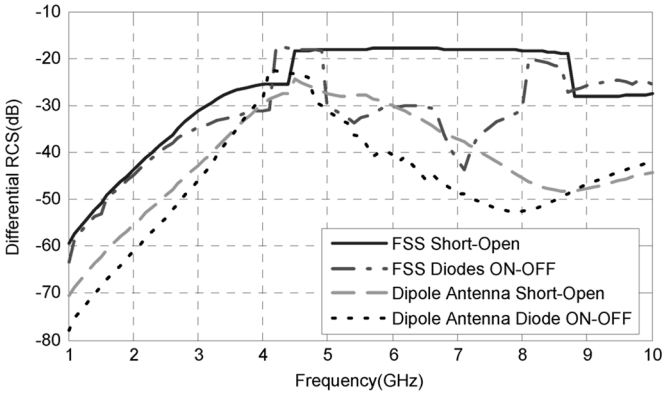

Fig. 15. Comparison of the differential RCS between the FSS and a dipole antenna between Short-Open states and between Diodes ON-OFF states.

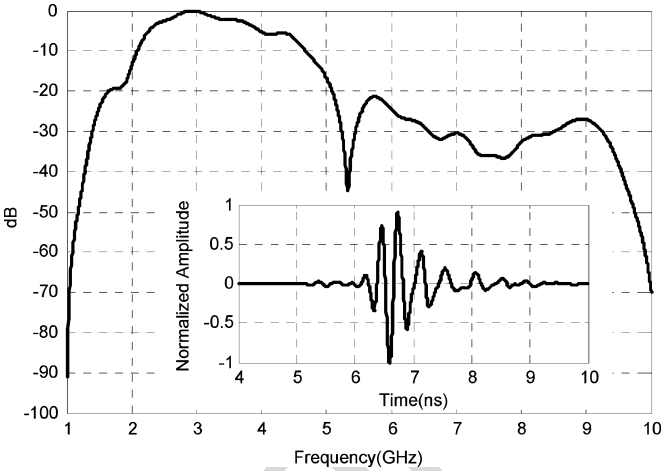

Fig. 16. Frequency response of the transfer function. In the inset figure the measured time response.

about 0.8 Vpp amplitude, 4.4 GHz center frequency and 125 ps duration.

In order to predict the modulating index of the OOK modulation from the simulated RCS, the overall transfer function is needed $H_{\mathrm{TX}}(\omega)H_{\mathrm{CH}}(\omega)H_{\mathrm{RX}}(\omega)$. Using the method described in Section II, the transfer function (when measured with the antennas oriented face-to-face) can be obtained from the received signal. In our case, two identical Vivaldi antennas excited with microstrip-to-slot line transition are used as TX and RX antennas. These antennas are often used in UWB applications and present moderate gain and low distortion. The antennas are a scaled version of the antenna presented in [32]. These antennas have a VSWR typically better than 2 and a bandwidth between 1.4 and 8.8 GHz. Fig. 16 shows the normalized transfer function as a function of the frequency. The inset plot shows the normalized time-domain measured signal $(s_{\mathrm{cal}}(t))$. There is a clear band-pass effect as a consequence of the combination of the pulse band-pass spectrum and the antenna transfer function. Thus, the amplitude of the reflected pulse on the FSS depends on the RCS apodized by this band-pass function. Fig. 17 shows the time-domain signal reflected by the FSS for different load conditions. These signals are obtained by the Fourier inverse transform of the product of the backscattered field obtained from Figs. 7 and 10, and the transfer function given in Fig. 16. Fig. 18 shows that a simple envelope detector (for instance by the modulus of the Hilbert transform of the time-domain signal) can be used to demodulate the OOK signal. As explained in Section II, the diodes parasitic elements reduce the transparence of the FSS. An amplitude modulating index close to 0.5 can be achieved between short and open circuit load conditions. However, due to the reduction in the FSS transparence for the state with the diodes in OFF, the modulating index is close to 0.85 between the ON and OFF states. In order to interpret these results, the FSS must be viewed as a bandpass filter. The amplitude of the reflected energy and in consequence the amplitude of the reflected pulse is higher for short load conditions and when the diodes are ON. For these cases, the resonance frequency of the FSS has approximately the same frequency than the peak of the spectrum of the pulse. Whereas in the case of diodes OFF and specially for open load condition due to the shift of the FSS resonance frequency, the reflected energy is smaller than on short and diodes ON cases. So, the level of the reflected signal is a function of the offset between the FSS frequency pass bands between states.

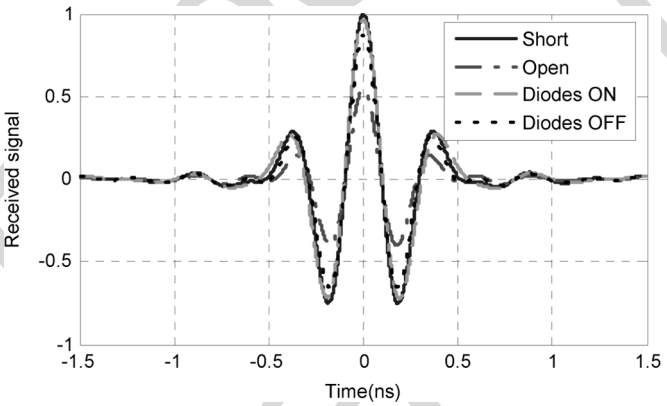

Fig. 17. Simulated normalized received signal as function of time for different load conditions.

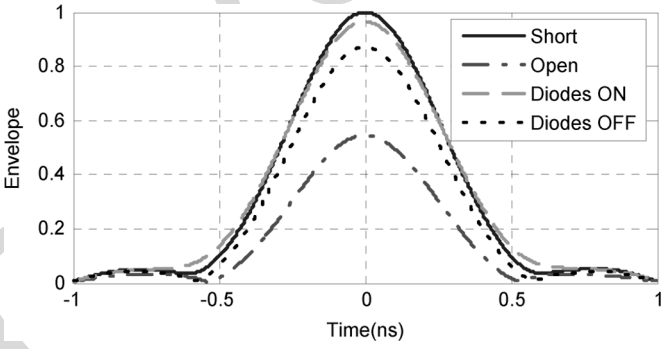

Fig. 18. Simulated normalized envelope of the time-domain response of tag.

Figs. 19 and 20 show the measured reflected signal by the tag for tag-to-reader distances of 0.5 and 1.5 m, respectively. In both cases, the radar receives 512 time samples spaced approximately 30 ps between each sample. A time offset can be configured to choose the measurement range window. At the top of Figs. 19 and 20 the envelope of the raw signal is shown. The presence of strong clutter from the ground reflections is observed because the measurements are done in a real scenario, not

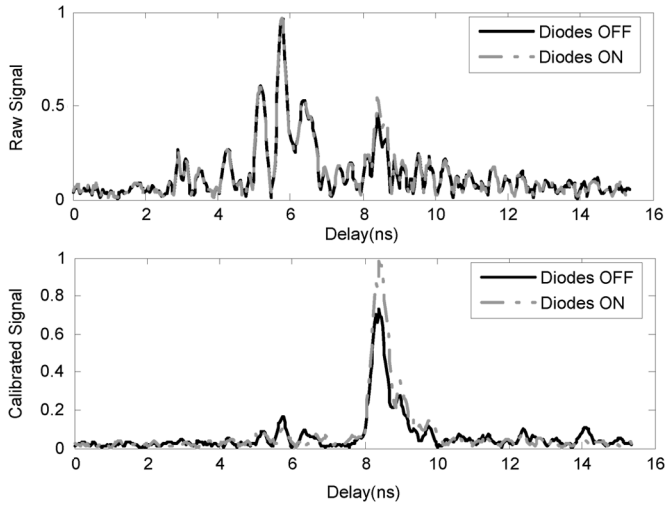

Fig. 19. Envelope of the measured signal (top), and the envelope of the signal after background removed (bottom) from the tag-to-reader distance of 0.5 m.

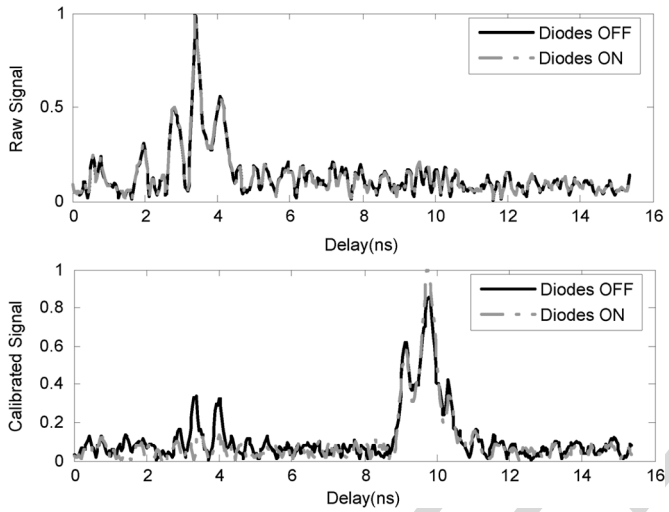

Fig. 20. Envelope of the measured signal (top), and the envelope of the signal after background removed (bottom) from the tag-to-reader distance of 1.5 m.

in an anechoic chamber. After removing the background previously measured (measurement without the tag), the tag response can be clearly viewed at the bottom of Figs. 19 and 20. The measured modulating index is very close to the simulated one (about 0.8).

In order to evaluate the distortion of the received pulse due to the FSS, Fig. 21 compares the measured received pulses reflected by a large metal plate (assumed as the reference) and the reflected pulse by the FSS in its two states. The same pulse generator than in Fig. 16 has been used. It can be seen that the shape is not much changed. The fidelity factor [33] is often used to measure the distortion due to shape changes. In this case, taking as the reference the pulse reflected by the metal plate, the fidelity factors are 0.94 and 0.98 for the OFF and ON states, respectively. Therefore, the FSS can support (with low distortion) typical UWB pulses with a centre frequency between 3 and 4 GHz.

The next figures show the measured signal when a sequence of bits is sent by the tag modulating the backscattered signal.

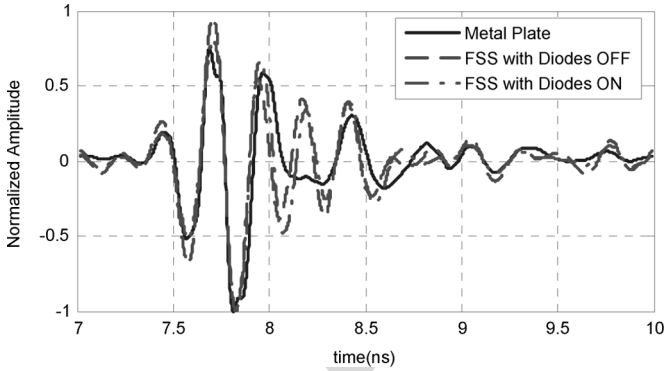

Fig. 21. Measured time domain received signal for a metal plate target and the FSS with Diodes OFF and ON.

The bit 0 is obtained when the diodes are OFF and the bit 1 when the diodes are ON. At the top of Fig. 22 the envelope of the received signal is shown. To demodulate the sequence, it is possible to use a simple threshold comparator. However, this method requires the adaptive estimation of the threshold, since it changes with the tag-to-reader distance. In addition, as explained before, this method needs to solve the problem of the estimation of the background in real RFID scenarios. An improvement can be obtained if differential coding is used. Assuming that the tag remains in repose, the first bit is zero because the diodes are OFF. Then, the measured waveform for the first bit can be used as an estimation of the background that will be subtracted in the next bits. Fig. 22 (bottom) shows the envelope of the differential signal. Thanks to the high repeatability in the bit states a simple threshold can be obtained to demodulate the sequence (i.e., by setting the threshold to equal the half of the maximum normalized envelope amplitude). Figs. 23 and 24 show an image of the envelope as a function of the delay for each bit of the sequence, before and after subtracting the first bit waveform (differential schema), respectively. It can be observed that the "0" and "1" signals are more distinguishable between each other when the differential schema is applied.

V. Conclusion

In this work, the basic theory of operation of UWB RFID using active FSS as tags has been presented. The results show that is possible to modulate the amplitude of the time-domain backscattered signal using a simple FSS. The FSS is composed by printed dipoles loaded with PIN diodes as switching elements. In contrast with traditional backscattering methods where the tag or antenna mode is modulated, in this work the total radar cross section of the surface (equivalent to the structural mode in antennas) is modulated. The RCS is proportional to the area and increases with the wavelength facilitating the tag detection. The index of modulation depends largely on the diode parasitic elements. However, the detection of the backscattered signal can be done using differential schemas that remove clutter interferences in the signal without using advanced calibration or threshold estimation techniques. A semipassive tag has been designed as a proof of concept. The tag integrates a low-power microcontroller. The tag remains in sleep mode with ultra-low power consumption until a 2.45

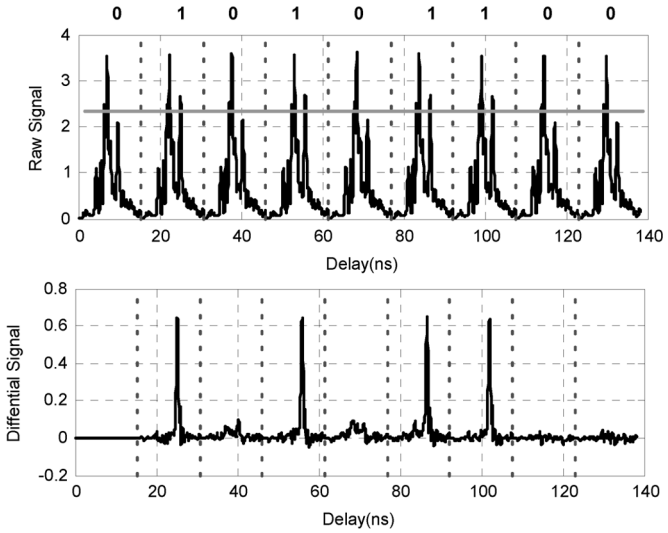

Fig. 22. Envelope of the received signal (top figure) and the differential signal obtained subtracting the waveform for the first bit (bottom figure), for the bit sequence shown in the top. The tag-to-reader distance is 0.5 m.

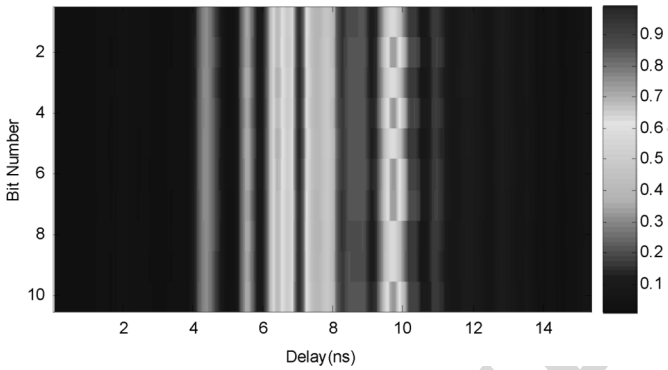

Fig. 23. Image of the envelope of the received signal for the same bit sequence of Fig. 22.

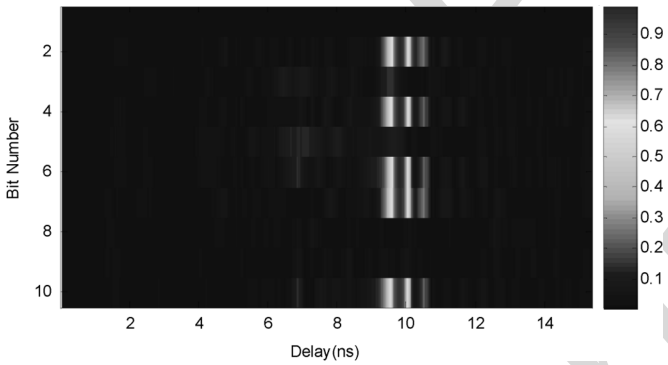

Fig. 24. Image of the envelope of the differential signal for the same bit sequence of Fig. 22.

GHz modulated signal wakes up the tag. The wake-up circuit is based on a diode detector and it uses the microcontroller comparator to reduce the number of parts and the consumption. Then, the microcontroller transmits the stored data or identification data modulating the RCS of the FSS. An experimental setup based on a low-power UWB radar is used as the reader. These results open the door to use FSS technologies in UWB RFID applications such ultra-low cost and ultra-low power environmental sensor networks.

Ranging and positioning are other benefits that UWB scheme brings to the system. It can be a powerful candidate for asset monitoring and positioning applications. The use of backscattering system allows reduce the power compared with active or semi passive tags based on ASK or FSK transmitters. In addition, these tags can be read by low power UWB radar in contrast with narrow band traditional passive RFID systems where high transmitted power and high power consuming readers are required.

ACKNOWLEDGMENT

The authors would like to thank Prof. Josep Parrón from Telecommunication and System Engineering Department of the Universitat Autònoma de Barcelona (UAB) for his support with the electromagnetic simulations with FEKO.

REFERENCES

[1] R. J. Fontana, "Recent system applications of short-pulse ultra-wideband (UWB) technology," *IEEE Trans. Microw.Theory Tech.*, vol. 52, no. 9, pp. 2087–2104, Sep. 2004.

[2] K. Finkenzeller, *RFID Handbook*, 3rd ed. Hoboken, NJ, USA: John Wiley & Sons, 2010.

[3] S. Preradovic, I. Balbin, N. C. Karmakar, and G. F. Swiegers, "Multiresonator-based chipless RFID systemfor low-cost item tracking," *IEEE Trans. Microw. Theory Tech.*, vol. 57, no. 5, pp. 1411–1419, May 2009.

[4] D. Dardari and R. D'Errico, "Passive ultrawide bandwidth RFID," in *Proc. IEEE Global Telecommun. Conf. (GLOBECOM)*, 2008, pp. 1–6.

[5] S. Hu, Y. Zhou, C. L. Law, and W. Dou, "Study of a uniplanar monopole antenna for passive chipless UWB-RFID localization system," *IEEE Trans. Antennas Propag.*, vol. 58, no. 2, pp. 271–278, Feb. 2010.

[6] A. Ramos, A. Lázaro, D. Girbau, and R. Villarino, "Time-domain measurement of time-coded UWB chipless RFID tags," *Progress Electromagnetics Res.—PIER*, vol. 116, pp. 313–331, 2011.

[7] A. Lazaro, A. Ramos, D. Girbau, and R. Villarino, "Chipless UWB RFID tag detection using continuous wavelet transform," *IEEE Antennas Wireless Propag. Lett.*, vol. 10, pp. 520–523, 2011.

[8] S. Preradovic, N. Karmakar, and M. Zenere, "UWB chipless tag RFID reader design," in *Proc. IEEE Int. Conf. RFID-Technol. Appl.* , Guangzhou, China, June 17–19, 2010.

[9] A. Lazaro, D. Girbau, and D. Salinas, "Radio link budgets for UHF RFID on multipath environments," *IEEE Trans. Antennas Propag.*, vol. 57, no. 4, pp. 1241–1251, Apr. 2009.

[10] A. Lazaro, D. Girbau, and R. Villarino, "Effects of interferences in UHF RFID systems," *Progress Electromagn. Res.—PIER*, vol. 98, pp. 425–443, 2009.

[11] J. Lorenzo, D. Girbau, A. Lázaro, and R. Villarino, "Read range reduction in UHF RFID due to antenna detuning and gain penalty," *Microw. Opt. Technol. Lett.*, vol. 53, no. 1, pp. 144–148, 2011.

[12] B. A. Munk, *Frequency Selective Surfaces*. New York, NY, USA: Wiley, 2000.

[13] B. A. Munk, R. G. Kouyoumjian, and L. Peters, "Reflection properties of periodic surfaces of loaded dipoles," *IEEE Trans. Antennas Propag.*, vol. AP-19, no. 5, pp. 612–617, Sep. 1971.

[14] P. S. Neelakanta, A. K. Stampalia, and D. De Groff, "An actively-controlled microwave reflecting surface with binary-pattern modulation," *Microw. J.*, vol. 46, no. 12, pp. 22–35, Dec. 2003.

[15] G. Marrocco, "RFID grids: Part I—Electromagnetic theory," *IEEE Trans. Antennas Propag.*, vol. 59, no. 3, pp. 1019–1026, Mar. 2011.

[16] M. Ghavami, L. B. Michael, and R. Kohno, *Ultra Wideband Signals and Systems in Communication Engineering*. Hoboken, NJ, USA: Wiley, 2004.

[17] ***[AU: Please provide more information.]*** [Online]. Available: http://www.novelda.no/content/radar-icsNovelda AS, Garverivegen 2,NO-3850 Kviteseid, Norway, Website:

[18] J. Ansari, D. Pankin, and P. Mähönen, "Radio-triggered wake-ups with addressing capabilities for extremely low power sensor network applications," *Int. J. Wireless Inf. Netw.*, vol. 16, pp. 118–130, 2009.
[19] G. Vannucci, A. Bletsas, and D. leigh, "A software. defined radio system for backscatter sensor networks," *IEEE Trans. Wireless Commun.*, vol. 7, no. 6, pp. 2170–2179, Jun. 2008.
[20] A. Ferrer-Vidal, A. Rida, S. Basat, L. Yang, and M. M. Tenzeris, "Intergration of sensors and RFID's on ultra-low-cost paper-based substrates for wirelss sensor networks applications," presented at the 2006 2nd Workshop Wireless Mesh Netw. (WiMesh 2006), .
[21] R. E. Collin and F. J. Zucker, *The Receiving Antenna, Antenna Theory*. New-York, NY, USA: McGraw-Hill, 1969, part 1.
[22] R. B. Green, The General Theory of Antenna Scattering ElectroScience Laboratory Columbus, OH, USA, Tech. Rep. 1223-17, 1963.
[23] P. V. Nikitin, K. V. S. Rao, S. F. Lam, V. Pillai, R. Martinez, and H. Heinrich, "Power reflection coefficient analysis for complex impedances in RFID tag design," *IEEE Trans. Microw. Theory Tech.*, vol. 53, no. 9, pp. 2721–2725, Sep. 2005.
[24] S. Licul and W. A. Davis, "Unified frequency and time-domain antenna modeling and characterization," *IEEE Trans. Antennas Propag.*, vol. 53, no. 9, pp. 2882–2888, Sep. 2005.
[25] Y. Duroc, T.-P. Vuong, and S. Tedjini, "A time/frequency model of ultrawideband antennas," *IEEE Trans. Antennas Propag.*, vol. 55, no. 8, pp. 2342–2350, Aug. 2007.
[26] ***[AU: Please provide more info.]*** [Online]. Available: http://www.microchip.com/wwwproducts/Devices.aspx?dDocName=en538963#1PIC16(L)F1826/27 18/20/28-Pin Flash MCU with nanoWatt XLP, 2011 Microchip Technology Inc. Available in:
[27] ***[AU: Please provide more info.]*** Application Note AN 1089 Designing Detectors for RF ID Tags, Avago Technologies.
[28] M. N. Jazi and T. A. Denidni, "Frequency selective surfaces and their applications for nimble-radiation pattern antennas," *IEEE Trans. Antennas Propag.*, vol. 58, no. 7, pp. 2227–2237, Jul. 2010.
[29] ***[AU: Please provide more info.]*** 2004, BAP51-03. General purpose PIN diode, NXP.
[30] Application Note 1330, HMPP-3865 MiniPAK PIN Diode High Isolation SPDT Switch Design for 1.9 GHz and 2.45 GHz Applications, Avago Technologies.
[31] H. A. Hjortland, D. T. Wisland, T. S. Lande, C. Limbodal, and K. Meisal, "Thresholded samplers for UWB impulse radar," in *Proc. IEEE Int. Symp. Circuits Syst. (ISCAS 2007)*, New Orleans, LA, USA, May 27–30, 2007, pp. 1210–1213.
[32] A. Lazaro, D. Girbau, and R. Villarino, "Weighted centroid method for breast tumor localization using an UWB RADAR," *Progress Electromagn. Res. B*, vol. 24, pp. 1–15, 2010.
[33] A. Mehdipour, K. Mohammadpour-Aghdam, and R. Faraji-Dana, "Complete dispersion analysis of Vivaldi antenna for ultra wideband applications," *Progress Electromagn. Res., PIER 77*, pp. 85–96, 2007.

Antonio Lázaro (M'07) was born in Lleida, Spain, in 1971. He received the M.S. and Ph.D. degrees in telecommunication engineering from the Universitat Politècnica de Catalunya (UPC), Barcelona, Spain, in 1994 and 1998, respectively.

He then joined the faculty of UPC, where he currently teaches a course on microwave circuits and antennas. In July 2004. he joined the Department of Electronic Engineering, Universitat Rovira i Virgili, Tarragona, Spain. His research interests are microwave device modeling, on-wafer noise measurements, monolithic microwave integrated circuits (MMICs), low phase noise oscillators, MEMS, and microwave systems.

Angel Ramos received the B.S. degree in telecommunication engineering and the M.S. degree in electronic engineering from Universitat Rovira i Virgili (URV), Tarragona, Spain, in 2010 and 2011, respectively. He is currently working toward the Ph.D. degree within the Department of Electronics, Electrics and Automatics Engineering at URV.

David Girbau (M'04) received the B.S. degree in telecommunication engineering, the M.S. degree in electronics engineering, and the Ph.D.degree in telecommunication from Universitat Politècnica de Catalunya (UPC), Barcelona, Spain, in 1998, 2002, and 2006, respectively.

From February 2001 to September 2007, he was a Research Assistant with the UPC. From September 2005 to September 2007, he was a Part-Time Assistant Professor with the Universitat Autònoma de Barcelona (UAB). Since October 2007, he has been a Full-Time Professor at Universitat Rovira i Virgili (URV). His research interests include microwave devices and systems, with emphasis on UWB, RFIDs, and RF-MEMS.

Ramon Villarino received the B.Sc. degree in telecommunications eechnical engineering from the Ramon Llull University (URL), Barcelona, Spain, in 1994, the M.Sc. degree in senior telecommunications engineering from the Polytechnic University of Catalonia (UPC), Barcelona, Spain, in 2000, and the Ph.D.degree from the UPC, in 2004.

During 2005–2006, he was a Research Associate at the Technological Telecommunications Center of Catalonia (CTTC), Barcelona, Spain. He worked at the Autonomous University of Catalonia (UAB) from 2006 to 2008 as a Researcher and Assistant Professor. Since January 2009, he has been a Full-Time Professor at Universitat Rovira i Virgili (URV). His research interests include radiometry, microwave devices, and systems, based on UWB, RFIDs, and frequency selective structures using MetaMaterials (MM).